Tree allocation dynamics beyond heat and hot drought stress reveal changes in carbon storage, belowground translocation and growth

Romy Rehschuh[1] (iD), Stephanie Rehschuh[1], Andreas Gast[1], Andrea-Livia Jakab[1], Marco M. Lehmann[2] (iD), Matthias Saurer[2] (iD), Arthur Gessler[2,3] (iD) and Nadine K. Ruehr[1] (iD)

[1]Karlsruhe Institute of Technology (KIT), Institute of Meteorology and Climate Research – Atmospheric Environmental Research (IMK-IFU), Garmisch-Partenkirchen 82467, Germany;

[2]Swiss Federal Research Institute WSL, Research Unit Forest Dynamics, Birmensdorf 8903, Switzerland; [3]Department of Environmental System Sciences, ETH Zurich, Zurich 8092, Switzerland

Summary

- Heatwaves combined with drought affect tree functioning with as yet undetermined legacy effects on carbon (C) and nitrogen (N) allocation.
- We continuously monitored shoot and root gas exchange, $\delta^{13}CO_2$ of respiration and stem growth in well-watered and drought-treated *Pinus sylvestris* (Scots pine) seedlings exposed to increasing daytime temperatures (max. 42°C) and evaporative demand. Following stress release, we used $^{13}CO_2$ canopy pulse-labeling, supplemented by soil-applied ^{15}N, to determine allocation to plant compartments, respiration and soil microbial biomass (SMB) over 2.5 wk.
- Previously heat-treated seedlings rapidly translocated ^{13}C along the long-distance transport path, to root respiration (R_{root}; 7.1 h) and SMB (3 d). Furthermore, ^{13}C accumulated in branch cellulose, suggesting secondary growth enhancement. However, in recovering drought-heat seedlings, the mean residence time of ^{13}C in needles increased, whereas C translocation to R_{root} was delayed (13.8 h) and ^{13}C incorporated into starch rather than cellulose. Concurrently, we observed stress-induced low N uptake and aboveground allocation.
- C and N allocation during early recovery were affected by stress type and impact. Although C uptake increased quickly in both treatments, drought-heat in combination reduced the above–belowground coupling and starch accumulated in leaves at the expense of growth. Accordingly, C allocation during recovery depends on phloem translocation capacity.

Introduction

The Earth's forests play an important role in the global carbon (C) cycle by removing a large amount of CO_2 from the atmosphere (Pan *et al.*, 2011; Le Quéré *et al.*, 2018). Worldwide, forests store about 653 billion tC, which approximates to anthropogenic CO_2 emissions of approximately 75 yr (Klein & Schulz, 2011). However, the ability of forests to regulate C and nutrient cycling is tightly linked to climatic conditions (Rennenberg *et al.*, 2006), which are projected to change rapidly within the 21st Century (Coumou *et al.*, 2013; IPCC, 2018). Heatwaves under wet conditions, but also hot droughts associated with high vapor pressure deficit (VPD), have become more common (Hao *et al.*, 2013; Stéfanon *et al.*, 2014), and thus intensify climatic stress on forests globally (Grossiord *et al.*, 2020; McDowell *et al.*, 2020).

Heatwaves directly impact plant physiological processes by influencing enzymatic activity and membrane integrity (Schrader *et al.*, 2004; Rennenberg *et al.*, 2006; Sage *et al.*, 2008), as well

as mitochondrial and dark respiration (Teskey *et al.*, 2015). The impacts of heatwaves depend on water availability (Ruehr *et al.*, 2016) and heat combined with drought affect plants even more because evaporative demand intensifies (Kumarathunge *et al.*, 2020). Trees are able to regulate water loss by closing stomata, therefore limiting tree internal pressure and dehydration (Tyree & Sperry, 1989). However, reduced stomatal conductance limits evaporative leaf cooling, leading to higher leaf temperatures (Birami *et al.*, 2018; Drake *et al.*, 2018). Furthermore, it decreases CO_2 uptake via photosynthesis (Rennenberg *et al.*, 2006; Ruehr *et al.*, 2016; Birami *et al.*, 2018), which can influence C and nitrogen (N) allocation dynamics (Ruehr *et al.*, 2009; Blessing *et al.*, 2015; Schönbeck *et al.*, 2020) and growth rates (Bauweraerts *et al.*, 2014; Teskey *et al.*, 2015; Ruehr *et al.*, 2016). A negative whole-plant C balance might arise if respiration costs for metabolic maintenance exceed C assimilation rates. Consequently, the metabolism needs to be sustained by nonstructural carbohydrates (NSC) and other C storage pools. A

depletion of these pools might affect the ability of trees to recover and withstand subsequent stress events (McDowell *et al.*, 2008).

In addition, severe heatwaves and drought can result in metabolic impairment and functional damage, which clearly delays recovery pace (Ruehr *et al.*, 2019). Several stress legacy impacts have been reported, including decreased water transport as a consequence of persisting embolism, such as the blockage of xylem tracheids by air bubbles (Rehschuh *et al.*, 2020), reduced leaf biomass (Ruehr *et al.*, 2016; Timofeeva *et al.*, 2017), and reduced stem growth rates (Anderegg *et al.*, 2015), which have been linked to tree mortality processes (Trugman *et al.*, 2018). However, the underlying mechanisms, particularly the involvement of C assimilation and reserve mobilization in tree recovery, are far from being resolved (Martínez-Vilalta *et al.*, 2016). Little is known on C allocation patterns poststress, and the few studies on temperate tree species provide contrasting results. Although Zang *et al.* (2014) and Galiano *et al.* (2017) reported increased allocation of recent C aboveground, Hagedorn *et al.* (2016) and Joseph *et al.* (2020) found an enhanced belowground allocation, explained by root repair mechanisms.

Following stress release, a first step in gaining functionality is to upregulate photosynthesis. Recent assimilates might directly fuel metabolic demands and/or be added to carbohydrate storage (Galiano *et al.*, 2017). Long-distance transport from source to sink organs depends on sink demand and phloem transport capacity, including phloem loading and unloading (Lalonde *et al.*, 2003; De Schepper *et al.*, 2013; Sevanto, 2018). Phloem functionality, however, might be impaired by drought stress (Sevanto, 2014, 2018) even though it can eventually recover slowly once stress is released. This could hinder repair processes and regrowth of new functional tissue. To replace and regrow tissues lost or impaired during stress, C and N translocation from source to sink organs is essential (Rennenberg *et al.*, 2006; Gessler *et al.*, 2017). However, root N uptake can be reduced by drought and heat stress as a result of impaired root functioning (Fotelli *et al.*, 2004; Gessler *et al.*, 2005, 2017; Giri *et al.*, 2017). Despite this, information on the ability of trees to acquire and allocate N poststress is scarce. An imbalanced nutritional status can affect tissue growth, plant functioning and resistance. $^{13}CO_2$ and ^{15}N labeling allow a comprehensive picture to be formed of C and N allocation dynamics (Millard & Grelet, 2010; Epron *et al.*, 2012). ^{13}C labeling has been used in a variety of experiments, focusing particularly on impacts of seasonality (Dannoura *et al.*, 2011; Epron *et al.*, 2012), drought (Ruehr *et al.*, 2009; Zang *et al.*, 2014; Hagedorn *et al.*, 2016), elevated temperature (Blessing *et al.*, 2015; Drake *et al.*, 2019) and postdrought recovery (Zang *et al.*, 2014; Hagedorn *et al.*, 2016; Galiano *et al.*, 2017; Joseph *et al.*, 2020). ^{15}N tracer studies have evaluated the remobilization of N for seasonal growth (Millard & Grelet, 2010), and the capacity for N uptake and cycling depending on the internal N status (Dyckmans & Flessa, 2001; Schönbeck *et al.*, 2020), both during drought and heat stress (Dannenmann *et al.*, 2016; Aaltonen *et al.*, 2017; Giri *et al.*, 2017). However, studies on the combined C and N allocation dynamics post-heat and hot drought stress in temperate tree species are lacking, whereas this knowledge is crucial to improve our ability of predicting forests' resilience under climate change.

Scots pine (*Pinus sylvestris*), one of the most widespread conifers globally, recently has suffered from extreme climate events causing tree mortality (Buras *et al.*, 2018; Jaime *et al.*, 2019; Schuldt *et al.*, 2020). This has raised concerns about the resilience of this important timber species. Here, we exposed Scot pine seedlings to heat and hot drought scenarios late in the growing season after leaf elongation was completed, and constantly monitored above- and belowground gas exchange. We explicitly combined prolonged drought and heat stress as both have been observed to co-occur during summer extremes (De Boeck *et al.*, 2010). Following stress release, we applied $^{13}CO_2$ and ^{15}N labeling to closely follow C and N allocation patterns during a 2.5-wk recovery period. We were particularly interested in the different responses of above–belowground C and N cycling poststress, and addressed the following hypotheses: (1) translocation speed of recently assimilated C to belowground is enhanced post-heat, but delayed post-drought-heat; (2) recent C will be strongly invested into repair and growth, if stress impairment occurs; and (3) N uptake and allocation are strongly coupled with the C metabolism poststress.

Materials and Methods

Plant material and growth conditions

We obtained bare-rooted 3-yr-old *Pinus sylvestris* L. seedlings (Provenance 85 115, Franconia, Germany) from a tree nursery in March 2018. Seedlings were placed in separate pots (6.8 l) in C-free potting substrate, containing fine quartz sand (0.1–1.2 mm), medium-grained sand (1–2.5 mm), gravel (3–5.6 mm) and vermiculite (2 : 2 : 1 : 2). Additionally, 12 g long-term fertilizer (Osmocote® Exact Standard 5–6 M fertilizer 15-9-12 + 2MgO + TE; ICL Specialty Fertilizers, Geldermalsen, the Netherlands) was added per pot, and liquid fertilizer applied monthly for immediate nutrient supply (Compo® Complete, 6 + 4 + 6(+2) NPK(MgO); Hornbach, Bornheim, Germany). To mimic a typical forest soil microbial community, we applied a microbial wash by adding 8 l deionized water to 8 kg forest soil (Franconia, Germany), and soaked roots before potting. Finally, 100 ml of the liquid supernatant of the microbial wash was added to each pot after filtering (40-μm mesh). We also added 100 ml mycorrhiza inoculate (*Laccaria laccata*) per pot, inducing a mycorrhization rate of *c.* 50% after 6 months.

During plant acclimation and the whole experiment (see Fig. 1 (a) for timeline), seedlings were kept under controlled conditions in a glasshouse facility in Garmisch-Partenkirchen, Germany (708 m above sea level, lat. 47°28′32.9″N, long. 11°3′44.2″E). The glasshouse is equipped with highly UV-transmissive glass. Inside light was supplemented with sodium vapor lamps during daytime (T-agro 400W; Philips, Hamburg, Germany) and photosynthetic active radiation (PAR) recorded automatically (PQS1; Kipp&Zonen, Delft, the Netherlands).

Air temperature and relative humidity were adjusted to predefined conditions within the glasshouse compartment (CC600; RAM Regel- und Messtechnische Apparate GmbH, Herrsching, Germany), and measured automatically at canopy height
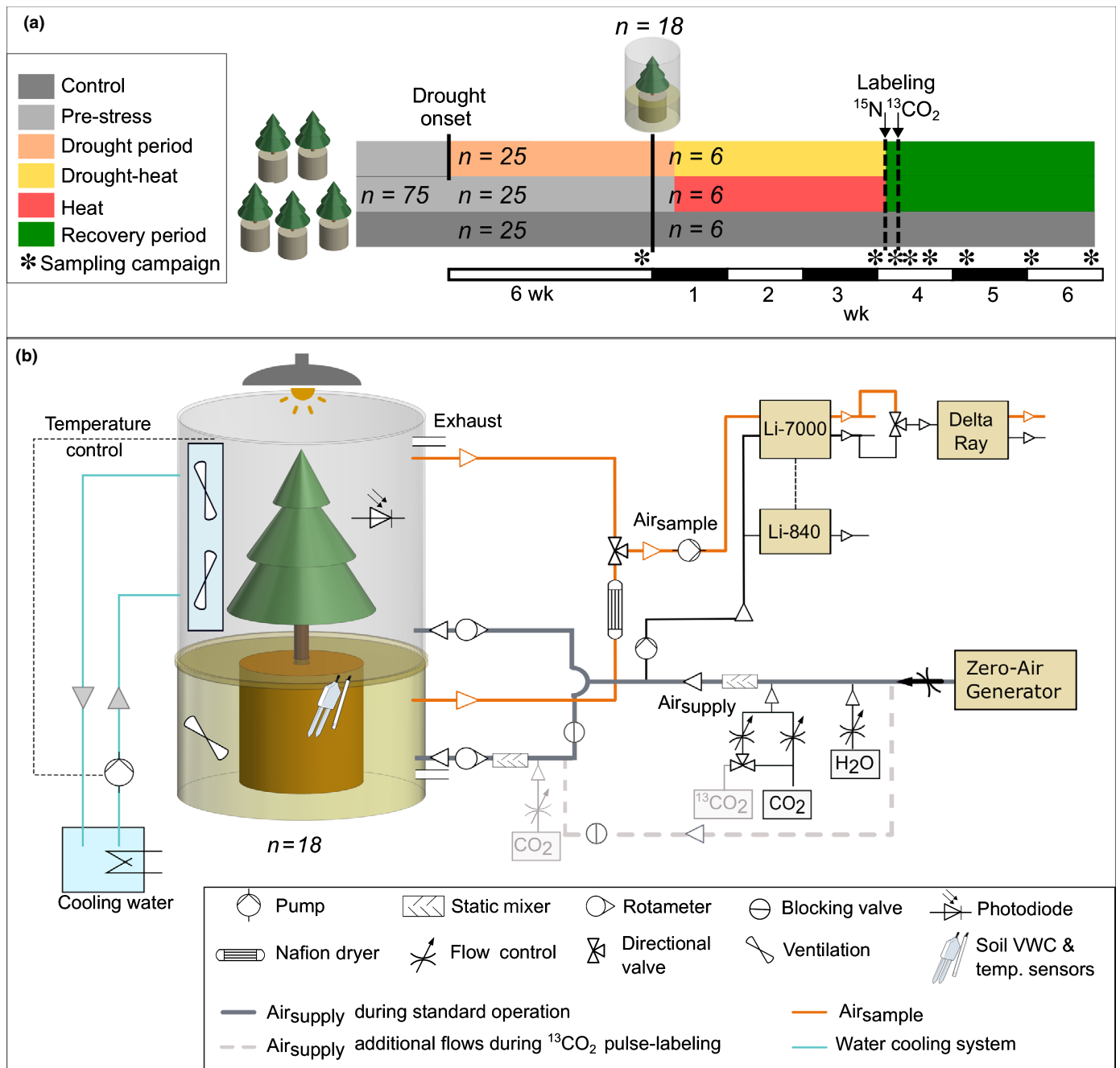
Fig. 1 Experimental timeline and schematic of the open gas-exchange chamber system (n = 18 chambers with seedlings and two empty chambers). (a) Scots pine seedlings were acclimated for 5 months after potting (light gray) before drought stress was initiated in randomly selected seedlings (orange). 6 wk later, six seedlings per treatment were randomly selected and transferred to the individual tree chambers where daytime heat stress was applied in the heat (middle bar) and the drought-heat (top bar) treatment. In order to keep the numbers of replicates sufficient, we were not able to investigate a drought-only treatment. Timing of labeling and manual sampling campaigns are depicted. (b) An exemplar individual tree chamber where arrows indicate the direction of air and water flow. Absolute CO_2 and H_2O concentrations were measured by a Li-840, connected to a Li-7000 for differential measurement of Air_{supply} and Air_{sample}. The associated $^{13}CO_2$ signature was measured by an isotope ratio infrared spectrometer (Delta Ray). Photosynthetic active radiation (PAR), air and soil temperature and soil moisture were continuously recorded and each seedling was equipped with an automatic drip irrigation system. Because seedlings were potted in C-free substrate and we corrected for potentially occurring microbial respiration (see Supporting Information Methods S2.2), the belowground flux was considered as root respiration (R_{root}).

(CS215; Campbell Scientific Inc., Logan, UT, USA). Seedlings were relocated frequently within the compartment. An individual drip irrigation system (Rain Bird, Azusa, CA, USA) served to adjust the watering automatically. During plant acclimation, all seedlings were watered daily to achieve a soil water content (SWC) close to field capacity (22%), monitored continuously (EC5; Meter Group AG, Munich, Germany). Temperature was on average 20.7°C (day 22.9°C, night 17.4°C). To mimic a

long-term drought after needle elongation was completed, irrigation was reduced in 25 seedlings on 2 August 2018, reaching a SWC ≈ 10% (Fig. S1). At the end of the 6-wk drought (before placing seedlings in the tree gas exchange chambers), needle water potential (Ψ_{Needle}) was -1.4 ± 0.05 MPa in drought compared to -0.6 ± 0.03 MPa in well-watered seedlings.

Experimental conditions On 18 September 2018, 18 seedlings ($n = 6$ drought, $n = 12$ well-watered) were transferred to individual gas exchange chambers placed in a glasshouse compartment and assigned to three treatments ($n = 6$ each): control (well-watered), heat (well-watered) and drought-heat (drought pre-stressed; see Table 1 for tree growth parameters).

We adjusted daytime temperature and vapor pressure deficit (VPD) based on a natural hot drought in 2003 and control conditions on 30-yr-averages in Franconia, Germany (Supporting Information Methods S1; Fig. S2). Following 5 d of acclimation, air temperature in the stress treatments was steadily increased by 2–3°C during daytime within 20 d to finally reach maximum temperatures of 41.5°C. Pre-defined maximum temperatures per period (Fig. 2; Table S1) were maintained for > 6 h daily (see Rehschuh & Ruehr, 2021), resulting in 14 d > 35°C. Daytime VPD increased alongside air temperature (Fig. 2b), but less in the heat compared to the drought-heat treatment as a consequence of increasing transpiration rates, affecting chamber humidity (Fig. S3). Note that night-time air temperatures and VPD did not differ between treatments owing to technical constraints. The importance of night-time temperatures has been analyzed for heatwaves in Europe and the increase in minimum temperatures reported to be much lower ($c.$ +3°C) than daytime temperatures ($c.$ +8°C; De Boeck et $al.$, 2010).

Soil compartments were passively cooled, hence mean soil temperature increased in all treatments, but remained < 30°C. An automated drip irrigation system allowed SWC to be maintained at field capacity in the control and heat treatment by watering four-times daily (300 ml in total; Fig. 2). Drought-heat treated seedlings were irrigated daily at 05:00 h (70 ml), whereas the amount was reduced steadily until SWC was $c.$ 5%. On 13 October 2018, stress was released, and drought-heat seedlings re-watered manually to field capacity (Fig. 2d). During the recovery phase, environmental parameters were adjusted to control conditions.

Individual tree gas exchange chambers

Chamber design and measurements We closely followed shoot and root gas exchange (H_2O and CO_2) and $\delta^{13}CO_2$ during stress and recovery using a custom-built tree chamber system (Birami et $al.$, 2020; Gattmann et $al.$, 2020; Fig. 1b). Briefly, each individual tree chamber ($n = 18$) consisted of a temperature-controlled (see Table S1) transparent shoot and opaque root compartment including either the shoot or the potted root part of one seedling. The compartments were gas-tight sealed from each other to prevent air flow from one compartment to the other (for details see Methods S2.1). Additionally, point dendrometers (DD-S; Ecomatik, Dachau, Germany) at 5–10 cm stem height were used to measure stem diameter half-hourly. Hourly-averaged stem diameter width above the initial measurements were interpreted as growth, values below as tree water deficit or rehydration.

The supply air ($\text{Air}_{\text{supply}}$) was constantly delivered to the chamber system at $c.$ 430 ppm CO_2 and 8 mmol H_2O during acclimation and recovery (see also Methods S2.2). During heat stress, [H_2O] was reduced to 4 mmol to avoid high humidity and condensation. $\delta^{13}CO_2$ of $\text{Air}_{\text{supply}}$ was kept constant at 0.28 ± 0.006‰ $\delta^{13}C$ (except during pulse-labeling). The isotopic ratios are expressed in δ notation (‰) relative to the international standard Vienna Pee Dee Belemnite (VPDB) for $\delta^{13}C$ and atmospheric N_2 for $\delta^{15}N$ (for solid samples only):

$$\delta^{13}C \text{ or } \delta^{15}N = \left(\frac{R_{\text{sample}}}{R_{\text{standard}}} - 1 \right) \cdot 1000‰ \qquad \text{Eqn 1}$$

(R, isotope ratio). Shoot compartments were supplied with $c.$ 13 l min^{-1} and root compartments with $c.$ 3 l min^{-1}. Sample air ($\text{Air}_{\text{sample}}$) was drawn back at 500 ml min^{-1}, and each compartment was measured once every 120 min. We organized the measurement sequence in order to avoid frequent switching between shoot and root compartments. Absolute H_2O and CO_2 concentrations were measured by a gas analyzer (Li-840; Li-cor, Lincoln, NE, USA), connected to a differential gas analyzer (Li-7000; Li-cor), allowing for determining the concentration differences in $\text{Air}_{\text{supply}}$ and $\text{Air}_{\text{sample}}$ in 10-s intervals over 80 s. The associated $\delta^{13}CO_2$ of $\text{Air}_{\text{supply}}$ and $\text{Air}_{\text{sample}}$ was determined by an isotope ratio infrared spectrometer (IRIS; Delta Ray; Thermo Fisher Scientific, Bremen, Germany) at 80 ml min^{-1}

Table 1 Tree properties and biomass of 3-yr-old *Pinus sylvestris* seedlings in the tree chambers, as well as soil microbial biomass (SMB) C and total dissolved nitrogen (TDN).

Treatment	Tree height (cm)	Stem diam. (mm)	Total biomass (g)	Branches (g)	Stem (g)	Root (g)	Needle (g)	Needle area (m^2)	SMB C (µg g^{-1} sdw)	TDN (mg kg^{-1} sdw)
Control	57.3 ± 1.8	16.4 ± 0.6	113.6 ± 4.5	21.8 ± 1.5	16.4 ± 1.0	36.3 ± 1.1	39.1 ± 2.9	0.17 ± 0.01	65.0 ± 6.8	159.7 ± 93.7
Heat	57.5 ± 1.9	15.9 ± 0.5	126.3 ± 12.8	23.4 ± 2.6	17.4 ± 2.0	35.8 ± 3.5	47.6 ± 4.6	0.18 ± 0.01	61.2 ± 3.6	83.8 ± 33.3
Drought-heat	58.1 ± 3.6	14.9 ± 0.4	107.6 ± 7.6	18.7 ± 1.2	14.0 ± 0.5	28.7 ± 1.9	46.1 ± 6.7	0.20 ± 0.03	26.2 ± 4.1	172.9 ± 76.7

Tree height, stem diameter, dry weight of total tree biomass, branches, stems, roots and needles, as well as needle area ($n = 6$ per treatment) were determined at the end of the experiment. SMB-C and TDN in the soil ($n = 3$ per treatment) are given for the end of the stress period. Data are given as treatment averages $\pm$ SE. A significant difference between treatments was observed for soil microbial biomass C in drought-heat only ($P < 0.01$; Kruskal–Wallis and Bonferroni *post hoc* test). sdw, soil dry weight.
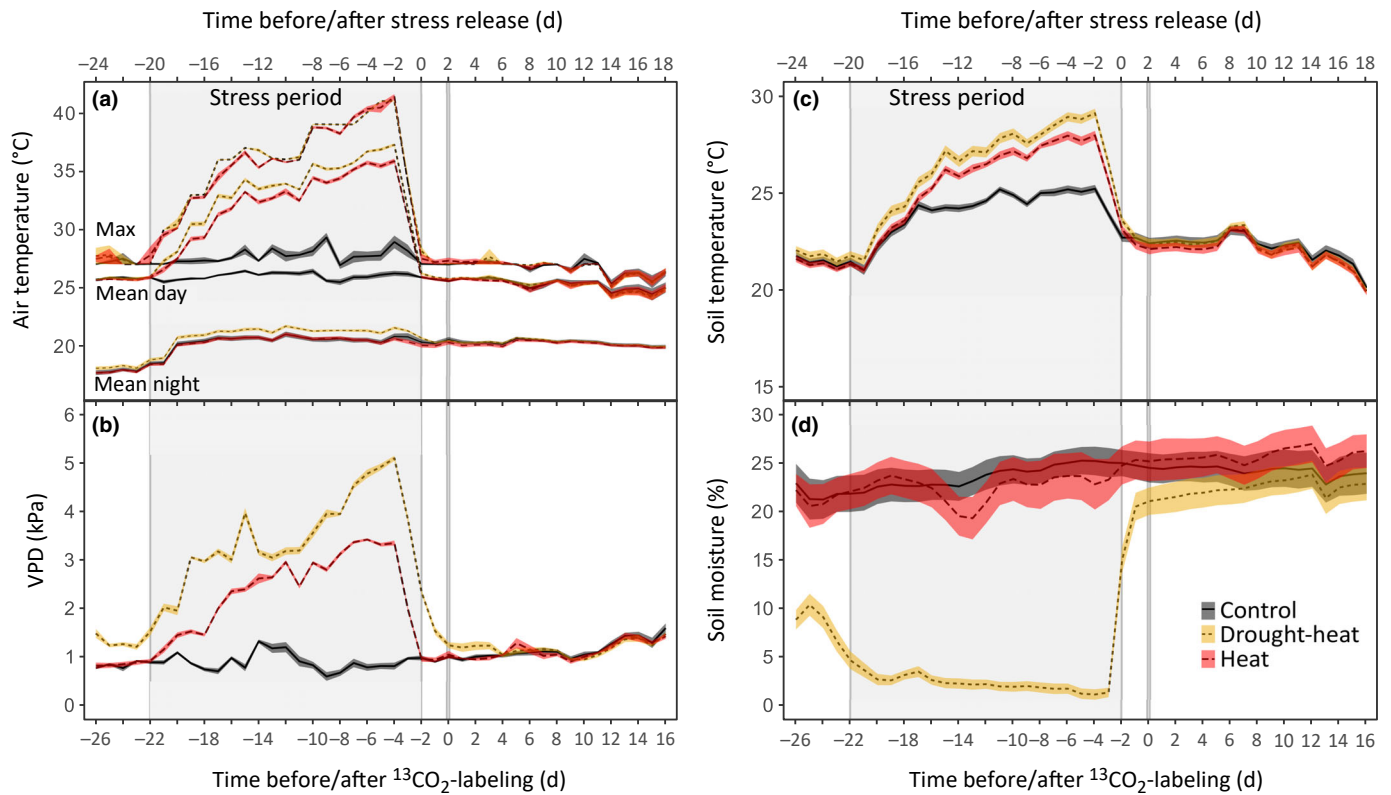
Fig. 2 Environmental conditions during the chamber experiment. Shown are (a) daytime (photosynthetic active radiation (PAR) > 100 μmol m^{-2} s^{-1}) and night-time mean and daily maximum air temperature, (b) daily daytime average vapor pressure deficit (VPD), (c) daily average soil temperature and (d) daily average soil moisture. Shown are treatment averages and shaded areas are ± SE ($n = 6$ per treatment). The gray boxes represent the stress period, and the vertical gray lines indicate the day of the experiment on which seedlings were $^{13}CO_2$ pulse-labeled (2 d after stress release). During the entire period, daytime average PAR was between 350 and 550 μmol m^{-2} s^{-1} in all treatments. Note that VPD in the drought-heat treatment was highest due to low tree transpiration rates. For diurnal patterns see Rehschuh & Ruehr (2021).

and measurements averaged over 60 s. Air$_{supply}$ was measured alternately between shoots and roots every 40 min, and remained relatively constant. Referencing was performed hourly using a commercially available reference gas with δ^{13}C = − 9.86 ± 0.3‰ (160 402; Thermo Fisher Scientific). The gas analyzers and the infrared spectrometer were calibrated before the experiment according to the manufacturer's recommendations.

In order to correct for offsets between Air$_{supply}$ and Air$_{sample}$ not caused by plant gas exchange, two chambers were operated without trees but containing pots with potting substrate. For calculations of gas exchange and isotopic signatures, see Methods S2.3 and Table S2.

$^{13}CO_2$ pulse-labeling and ^{15}N labeling

$^{13}CO_2$ pulse-labeling was performed on 15 October 2018, 2 d after stress release when C uptake of drought-heat seedlings was within 70% of control seedlings. Shoot compartments were pulse-labeled for 4 h during the period of highest photosynthetic activity, starting at 09:15 h. For this, we mixed 99% enriched $^{13}CO_2$ (364592-10L-EU; Sigma-Aldrich) directly to Air$_{supply}$ of shoot compartments (Fig. 1b), resulting in a [CO$_2$] of *c.* 400 ppm at 45 atom% ^{13}C (equals δ$^{13}CO_2$ of 75 000‰). The root compartments received nonenriched air (see Fig. S4). To

avoid memory effects on infrared spectroscopy measurements from highly enriched δ$^{13}CO_2$, we applied longer flushing (10 min) when switching between shoot and root compartments during and 24 h after labeling. We derived ^{13}C uptake per treatment, which compared well between a flux- and a biomass-based approach (Table 2).

C translocation rates were estimated from the time difference between the beginning of pulse-labeling and label appearance in root respiration (R_{root}), while considering stem length. Label appearance was defined individually per chamber based on a

Table 2 ^{13}C uptake by Scots pine seedlings during $^{13}CO_2$ pulse-labeling.

Treatment	Photosynthetic ^{13}C uptake (mg ^{13}C)	Needle biomass (mg ^{13}C)
Control	72.5 ± 5.1	61.6 ± 8.4
Heat	74.1 ± 5.1	68.4 ± 7.6
Drought-heat	50.0 ± 7.9	60.7 ± 11.1

Shown are data determined from gas exchange measurements for the 4-h labeling pulse and from excess ^{13}C of needle biomass sampled directly after labeling (for details see Supporting Information Methods S2.3). Data are treatment averages ± SE ($n = 6$). No significant differences between treatments were observed.

threshold calculated from pre-labeling variability of $\delta^{13}C$ ($SD_{pre-labeling}$) as follows: $2 \cdot 1.65 \cdot SD_{pre-labeling}$ (Salomón *et al.*, 2021).

To further derive information on the nutrient uptake capacity of roots and within-tree N allocation poststress, we applied double-labeled $^{15}NH_4^{15}NO_3$ (98% enriched; 366528-1G; Sigma-Aldrich) as follows. After seedlings were re-watered close to field capacity on 13 October 2018 at 05:00 h, we applied 170 ml of a 0.37 mM ^{15}N solution (5.1 mg ^{15}N) to each pot, evenly distributed around the stem.

Sample collection and preparation

In order to quantify NSC dynamics and the isotopic signatures of biomass (^{13}C and ^{15}N), water-soluble compounds (WSC), starch and cellulose (^{13}C), we subsampled needles, fine roots (diameter ≤ 2 mm) and branches of each seedling per individual tree chamber ($n = 18$). To minimize disturbance of continuous measurements, each seedling was sampled directly after gas exchange was quantified. Further, to assess pre-labeling variability, we took samples 1 d before stress release. Following $^{13}CO_2$ pulse-labeling, we sampled immediately after labeling (needles), 8 h, 15 h (needles), 27 h, 78 h, 7 d, 11 d and 16 d after the start of labeling, typically between 15:00 h and 16:00 h. Branches were separated immediately into xylem and phloem (including the cambium), except for branch cellulose determination. Root samples were rinsed with distilled and filtered water (dH_2O), and excess water removed. Plant biomass samples were immediately frozen in liquid N_2 and stored at $-80°C$ until freeze-drying (Alpha 24 LSC; Martin Christ Gefriertrocknungsanlagen GmbH, Osterode am Harz, Germany), and ground to fine powder (MM200; Retsch, Haan, Germany).

At the end of the experiment, each seedling was harvested and separated into needles, roots, branches and stems before oven-drying at 70°C for 48 h. DW (Table 1) was used to calculate ^{13}C and ^{15}N excess. Stem xylem DW was approximated for the outer tree ring based on stem xylem weight. Total leaf area per tree was derived from total needle biomass and pre-determined specific leaf area (g cm^{-2}; Li-3100; Li-cor).

Nonstructural carbohydrate analysis

We determined NSC concentrations from 10 mg plant material (needles, roots, branch phloem and xylem; $n = 5–6$ per treatment), thus soluble sugars (glucose, fructose and sucrose) and starch, according to Landhäusser *et al.* (2018). After extraction in 80% ethanol and specific enzymatic reactions, absorption was determined by a spectrophotometer at an absorption of 340 nm (Epoch 2; BioTek, Winooski, VT, USA; for details see Methods S3).

Water-soluble compounds, starch and cellulose extraction

For $\delta^{13}C$ analyses, WSC ($n = 6$) and starch ($n = 3$) were extracted from 40–60 mg dry homogenized biomass (needles, roots, branch phloem and xylem) following standard protocols (Richter *et al.*, 2009; Lehmann *et al.*, 2015; see Methods S4). WSC were extracted in 1.5 ml deionized water at 85°C for 30 min. Starch was enzymatically extracted from the remaining pellets using

heat-stable α-amylase. For $\delta^{13}C$ analysis of cellulose ($n = 5–6$), *c.* 15 mg cut plant material (branches, stems, fine roots) was step-wise extracted in Teflon filters using 5% NaOH and 7% acidified $NaClO_2$ at 60°C (Galiano *et al.*, 2017). Then, cellulose was homogenized by an Ultrasonic transducer (Laumer *et al.*, 2009).

Soil microbial biomass extraction

$\delta^{13}C$ of soil microbial biomass (SMB) was determined from soil samples taken close to roots ($n = 3$) during plant biomass sampling. Soil samples were immediately frozen at $-20°C$. To extract SMB, we applied a chloroform fumigation extraction method (Vance *et al.*, 1987; see Methods S5). $\delta^{13}C$ of fumigated and nonfumigated samples was determined by isotope ratio mass spectrometry, and total organic C by an infrared TOC analyzer (Dimatec, Essen, Germany). The $\delta^{13}C$ of SMB ($\delta^{13}C_{MB}$) was then calculated as follows:

$$\delta^{13}C_{MB}(‰) = \frac{\delta^{13}C_F \cdot C_F - \delta^{13}C_{NF} \cdot C_{NF}}{C_F - C_{NF}}, \qquad \text{Eqn 2}$$

(values from F, fumigated and NF, nonfumigated extracts). Total soil microbial C was calculated as (total C_F – total C_{NF})/0.45 (Vance *et al.*, 1987).

Isotope ratio mass spectrometry

In order to determine isotopic compositions and C and N contents of solid samples, *c.* 1 mg homogenized bulk material and cellulose, and *c.* 10 mg freeze-dried soil extracts were weighed into tin capsules. Liquid solutions of WSC and starch samples were pipetted into tin capsules and subsequently oven-dried at 70°C for 12 h, resulting in *c.* 0.5 mg DW. The samples were then combusted to CO_2 and N_2 in an elemental analyzer (EA1110 CHN; Carlo Erba, Milan, Italy) coupled to an isotope ratio mass spectrometer (Delta XL; Thermo Scientific, Bremen, Germany). For calibration, laboratory and international standards with known $\delta^{13}C$ and $\delta^{15}N$ were used, resulting in a precision of 0.2‰ for $\delta^{13}C$ and 0.3‰ for $\delta^{15}N$. Additionally, $\delta^{13}C$ and $\delta^{15}N$ of solid material and $\delta^{13}C$ of gas flux data were converted to atom%. For calculations of atom%, excess $^{13}C/^{15}N$ (amount of label in pools and biomass) and a ^{13}C mass balance see Methods S6.

Needle water potential and needle temperature

In order to assess drought severity, we measured Ψ_{Needle} of mature needles ($n = 6$ per treatment) before dawn and at noon-time using a pressure chamber (Model 1000; PMS Instruments, Albany, OR, USA). Measurements were performed at the end of stress and during initial and final recovery. We report the daily minimum Ψ_{Needle} here because irrigation took place in the morning, wherefore predawn Ψ_{Needle} was occasionally lower than mid-day Ψ_{Needle} in drought-treated seedlings.

Needle temperature was measured during the most severe stress and final recovery ($n = 6$ per treatment) around 13:00 h using an infrared camera (PI 450; Optris, Berlin, Germany). Images were analyzed using the manufacturer's software by

setting needle emissivity to 0.97 and adjusting background radiation according to air temperature.

Statistical data analysis

All data analyses and statistics were conducted in R v.3.6.1 (R Core Team, 2019). Stem increment rates were determined by fitting linear regression models to dendrometer data. Considering drought-heat seedlings, the model was fitted from 7 d after stress release until the end of the recovery period – when seedlings grew poststress and passed the pre-stress baseline. Significant differences between slopes of fitted lines per treatments were analyzed using least-squares means (package LSMEANS:LSTRENDS; Lenth, 2017). To test for significant differences between treatments at discrete time points (used for noncontinuous data and $^{13}C/^{15}N$ in plant tissues and compounds), we used the Kruskal–Wallis followed by the Bonferroni *post hoc* test for small sample sizes.

In order to analyze overall treatment effects per time period for continuous measurements (e.g. gas exchange, $\delta^{13}C$ of respiration, stem increment), linear-mixed effects models were applied (lme; LMERTEST package; Kuznetsova *et al.*, 2017). We assigned treatment and time period (pre-drought, initial and final stress, initial recovery until $^{13}CO_2$ labeling, recovery (labeling peak), recovery and final recovery) as fixed effect and chamber as random factor. The lme model with the lowest Akaike's information criterion corrected for small sample size (AICc) was chosen (Burnham & Anderson, 2002), and the *post hoc* Tukey's honestly significant difference (HSD) applied for multiple comparisons of means to determine differences between treatments (package EMMEANS; Lenth *et al.*, 2020).

We estimated the mean residence time (MRT) and half-life time (HLT) of the ^{13}C label in respiration, tissues and compounds by using the following exponential decay function:

$$N(t) = N_0 e^{-\lambda t}, \qquad \text{Eqn 3}$$

($N(t)$, $\delta^{13}C$ at time t; N_0, initial $\delta^{13}C$ at the labeling peak (here $t = 0$); and λ, decay constant). The MRT and HLT ($t_{1/2}$) were determined as follows:

$$\text{MRT} = \frac{1}{\lambda} \quad \text{and} \quad t_{1/2} = \frac{\log_e(2)}{\lambda} \qquad \text{Eqn 4}$$

We additionally fitted curves to ^{13}C dynamics of tissues and compounds to improve the visualization of ^{13}C trajectories over time. Models were selected based on the lowest AICc. We calculated the deviance to compare the fitted model to the null model, and determined the percentage explained by the best-fit model (reported here, Fuentes *et al.*, 2018). All statistical tests were considered significant if $P < 0.05$.

Results

Stress impacts and gas exchange recovery

Stress impacts on tree properties and biomass appeared small as drought was initiated after needle growth was completed, whereas SMB was reduced under drought-heat (Table 1). Gas exchange declined under drought as observed in lower net assimilation (A_{net}) and shoot dark respiration ($R_{shoot-night}$) compared to control seedlings (Tukey's HSD, $P > 0.1$; Fig. 3a,b). With increasing daytime air temperatures and VPD, A_{net}, $R_{shoot-night}$ and R_{root} declined strongly (Tukey's HSD, $P < 0.01$; see Table S3 for P-values per period). The larger stress impacts under drought-heat also were observed in low Ψ_{needle} (-2.70 ± 0.13 MPa; $P < 0.01$; Table 3), stem diameter shrinkage (Tukey's HSD, $P < 0.01$; Fig. 3d), and 4.6°C warmer maximum needle temperatures compared to the heat treatment ($P < 0.001$). By contrast, in well-watered heat-treated seedlings the effects of high temperatures were small, resulting in A_{net} declining to *c.* 70% of control values and slowly decreasing stem growth. Although R_{root} initially increased and then acclimated at higher temperatures (Tukey's HSD, $P > 0.1$; Table S3; Fig. 3), responses of $R_{shoot-night}$ were small as nighttime temperatures were kept at *c.* 20°C in all treatments.

Consequently, following stress release, A_{net}, $R_{shoot-night}$ and R_{root} recovered fast in heat seedlings (Fig. 3), and did not differ from the control during the recovery period (Tukey's HSD, $P > 0.1$). Additionally, stem growth rates increased above the control during the last week of recovery (heat: 0.043 mm d^{-1} vs control: 0.035 mm d^{-1}; $P < 0.001$).

Post-drought-heat, A_{net} and $R_{shoot-night}$ increased sharply, alongside increasing Ψ_{needle} (Table 3). A_{net} reached about 60% and $R_{shoot-night}$ 75% of control values 2 d poststress (Tukey's HSD, $P < 0.001$), with A_{net} recovering to *c.* 80% within the following 4 d (Tukey's HSD, $P < 0.05$), whereas $R_{shoot-night}$ recovered fully. R_{root} also increased and did not differ from the control during final recovery (Tukey's HSD, $P > 0.1$). Stem diameter width remained below pre-stress values until 6 d after stress release, marking the onset of secondary growth on Day 7. In the remaining recovery period, stem growth rates (0.066 mm d^{-1}) accelerated above control rates ($P < 0.001$).

Dynamics of ^{13}C in respiration, water-soluble compounds and soil microbial biomass

We closely monitored the dynamics of ^{13}C progression poststress (Fig. 4). In R_{root}, the first signal of ^{13}C arrived in the heat (7.06 $\pm$ 0.8 h), tightly followed by the control (8.3 $\pm$ 0.3 h) and *c.* 6 h later in the drought-heat treatment (13.8 $\pm$ 0.3 h; $P < 0.01$). This resulted in a 40% lower C translocation velocity in seedlings recovering from drought-heat compared to control seedlings ($P < 0.01$; heat: 4.14 $\pm$ 0.38 cm h^{-1}, control: 3.40 $\pm$ 0.20 cm h^{-1}, drought-heat: 1.98 $\pm$ 0.13 cm h^{-1}), alongside increased MRTs and HLTs (Table 4). The $\delta^{13}C$ peak in R_{root} was reached in both, the heat and control treatment 1 d after $^{13}CO_2$ labeling, that is, after 36 and 37 h (Fig. 4b). In drought-heat seedlings, the peak became apparent 24 h later and at a much lower intensity (866 $\pm$ 104‰ compared to 2352 $\pm$ 119‰ in control; Tukey's HSD, $P < 0.001$). Generally, we found re-occurring diurnal $\delta^{13}C$ peaks in R_{root} during night. By contrast, in $R_{shoot-night}$ the label peak occurred simultaneously in all treatments (at 04:00 h; *c.* 18 h after $^{13}CO_2$ labeling), but at different intensities and was lowest post-drought-heat (Fig. 4a). Further, $\delta^{13}C$ of $R_{shoot-night}$ leveled-
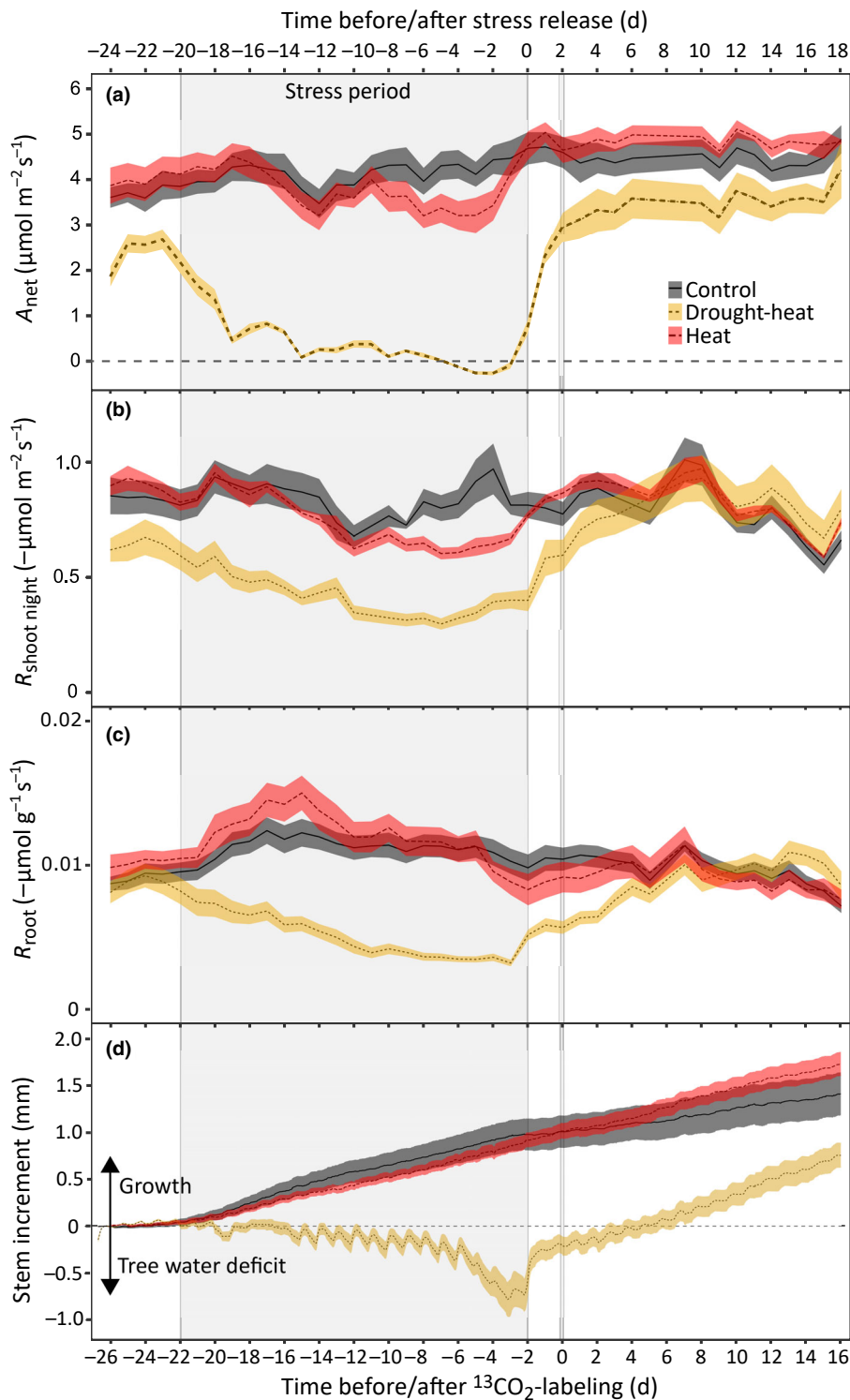
Fig. 3 Dynamics of treatment-specific gas exchange and stem diameter change in Scots pine. Shown are daily-averaged (a) net canopy assimilation (A_{net}), (b) shoot dark respiration ($R_{shoot-night}$) and (c) root respiration (R_{root}), as well as (d) half-hourly changes in stem increment. Data are treatment averages and shaded areas show $\pm$ SE ($n = 6$). The gray box represents the stress period, and with stress release ^{15}N was applied. The vertical gray line indicates when seedlings were $^{13}CO_2$ pulse-labeled (2 d after stress release). In (d), data above 0 indicate stem growth, and below 0, tree water deficit. Note that night-time temperatures did not differ between treatments.

off faster in the heat and control treatment, whereas the MRT was prolonged post-drought-heat (Table 4).

Respiration of recent assimilates is based on fast C pools such as WSC, including soluble sugars, sugar alcohols, organic acids and amino acids. Consistent with WSC supplying respiratory processes, WSC δ^{13}C initially declined fast in aboveground tissues of control and heat seedlings (Fig. 4; for ^{13}C excess, see Fig.

S5). In root WSC of these seedlings, highest δ^{13}C occurred 2 d after labeling (Fig. 4f), corresponding with the R_{root} label-peak. In heat seedlings, δ^{13}C in phloem and xylem WSC was larger compared to the other treatments within 1 d postlabeling (Fig. 4d,e), corresponding to a tendency of faster C translocation and lower MRT. In drought-heat seedlings, slower ^{13}C dynamics were reflected in longer MRTs of ^{13}C in WSC in most pools

Table 3 Minimum needle water potential (Ψ_{Needle}) and maximum and mean needle temperature of Scots pine seedlings at the end of stress, 1-d recovery and end of the recovery period.

Parameter	Treatment	End of stress	1-d recovery	End of recovery
Ψ_{Needle} (MPa)	Control	-0.56 ± 0.07	-0.44 ± 0.04	-0.61 ± 0.03
	Drought-heat	-2.70 ± 0.13	-0.98 ± 0.13	-0.66 ± 0.04
	Heat	-0.58 ± 0.08	-0.50 ± 0.07	-0.64 ± 0.02
Maximum needle temperature (°C)	Control	31.83 ± 0.45	–	28.09 ± 0.28
	Drought-heat	45.80 ± 0.43	–	28.23 ± 0.24
	Heat	41.16 ± 0.90	–	27.98 ± 0.16
Mean needle temperature (°C)	Control	29.56 ± 0.16	–	26.68 ± 0.31
	Drought-heat	44.29 ± 0.48	–	26.58 ± 0.34
	Heat	39.66 ± 0.59	–	26.12 ± 0.12

Data are treatment averages $\pm$ SE ($n = 6$).

(Table 4). The $\delta^{13}C$ dynamics of SMB showed a much slower trajectory that appeared uncoupled from the WSC dynamics (Fig. 4g; for ^{13}C excess, see Fig. S6).

C allocation to starch and cellulose

The $\delta^{13}C$ progression in starch and cellulose reflects the allocation of recent assimilates to storage and growth (Figs 5, S7, S8). Although drought reduced starch concentrations, starch increased in most tissues during recovery and exceeded the control at the end of the experiment (Fig. 5g–j). Contradictory, we found little treatment-specific differences in soluble sugar concentrations (Fig. S9). Recovering drought-heat seedlings strongly allocated recent C to starch and the $\delta^{13}C$ progression of needle starch revealed a longer MRT and HLT in drought-heat compared to heat and control seedlings (Fig. 5a; Table 4). By contrast, needle starch $\delta^{13}C$ of recovering heat seedlings decayed rapidly and MRT was lowest, displaying rapid translocation to sink tissues. This was congruent with higher $\delta^{13}C$ in branch cellulose, indicating fast allocation to growth (Fig. 5e). Control seedlings preferentially invested ^{13}C into root cellulose, whereas drought-heat seedlings incorporated little ^{13}C into cellulose. This indicates a delayed recovery of growth post-drought-heat, consistent with an apparent absence of stem increment during the initial 6 d of recovery (Fig. 3d).

^{13}C allocation dynamics and overall patterns

Treatment-specific dynamics of ^{13}C excess to tissue biomass were evident, with needle ^{13}C in drought-heat seedlings remaining elevated throughout the entire recovery period ($P < 0.05$), yet declining quickly in heat and control seedlings (Figs S10, S11). To summarize the ^{13}C allocation to respiration, plant tissues and compounds, we derived an isotopic mass balance. This included cumulative ^{13}C release via respiration (Fig. S12) and transfer to the SMB, and remaining ^{13}C in plant tissues/compounds 16 d after $^{13}CO_2$ pulse-labeling (i.e. 18 d after stress release; Fig. 6). A general pattern emerged, showing that in combination with drought, ^{13}C retention increased (Tukey's HSD, $P < 0.05$ drought-heat vs control) and ^{13}C release via R_{root} decreased during recovery (Tukey's HSD, $P < 0.01$ drought-heat). Although control seedlings favored ^{13}C investment into R_{root} and root

growth, this was not apparent in seedlings recovering from heat or drought-heat stress. In the heat treatment, we found preferred ^{13}C allocation to branch and stem cellulose, suggesting secondary woody growth. However, drought-heat seedlings hardly invested ^{13}C into growth, but NSC storage. In addition, a larger fraction of ^{13}C was respired aboveground (Figs 6, S12b), likely supplied by readily available ^{13}C in WSC. The reduced translocation belowground in drought-heat seedlings was further apparent from the low transfer of ^{13}C to SMB.

Tissue-specific dynamics of ^{15}N

The stress-induced inhibition of the above–belowground coupling was further reflected in a reduced ^{15}N uptake capacity of recovering drought-heat seedlings (Fig. 7d). Here, we report ^{15}N excess to account for differences in total N between treatments (Fig. S13). Clearly, recovering drought-heat seedlings assimilated significantly less ^{15}N than control seedlings (Fig. 7a–c). By contrast, ^{15}N dynamics of heat seedlings closely followed the trajectories of control seedlings, albeit missing a distinct ^{15}N peak in root tissues. The transient character of ^{15}N in roots and xylem was underlined by bell-shaped temporal trajectories. 9 d poststress, ^{15}N had been incorporated in needle and phloem tissues as curves leveled off.

Discussion

Stress impact and above–belowground coupling during recovery

Under well-watered conditions, the impacts of high daytime temperature ($< 43°C$) and vapor pressure (VPD) on *Pinus sylvestris* seedlings were small. Restricting the warming to daytime explains the missing temperature stimulation of $R_{shoot-night}$ and the rather small initial increase in R_{root}. Daytime heat stress in combination with drought resulted in highest leaf temperatures ($45.8°C$) and VPD, whereby stress impacts became severe and C loss exceeded C uptake. Remarkably, throughout the heatwave, we found that respiration acclimated closely following assimilation (Fig. 3). Such acclimation processes have been reported previously in response to warming (Jarvi & Burton, 2013; Birami *et al.*, 2020, 2021). For further information on temperature-related dynamics of gas exchange of the seedlings, see Rehschuh & Ruehr (2021).
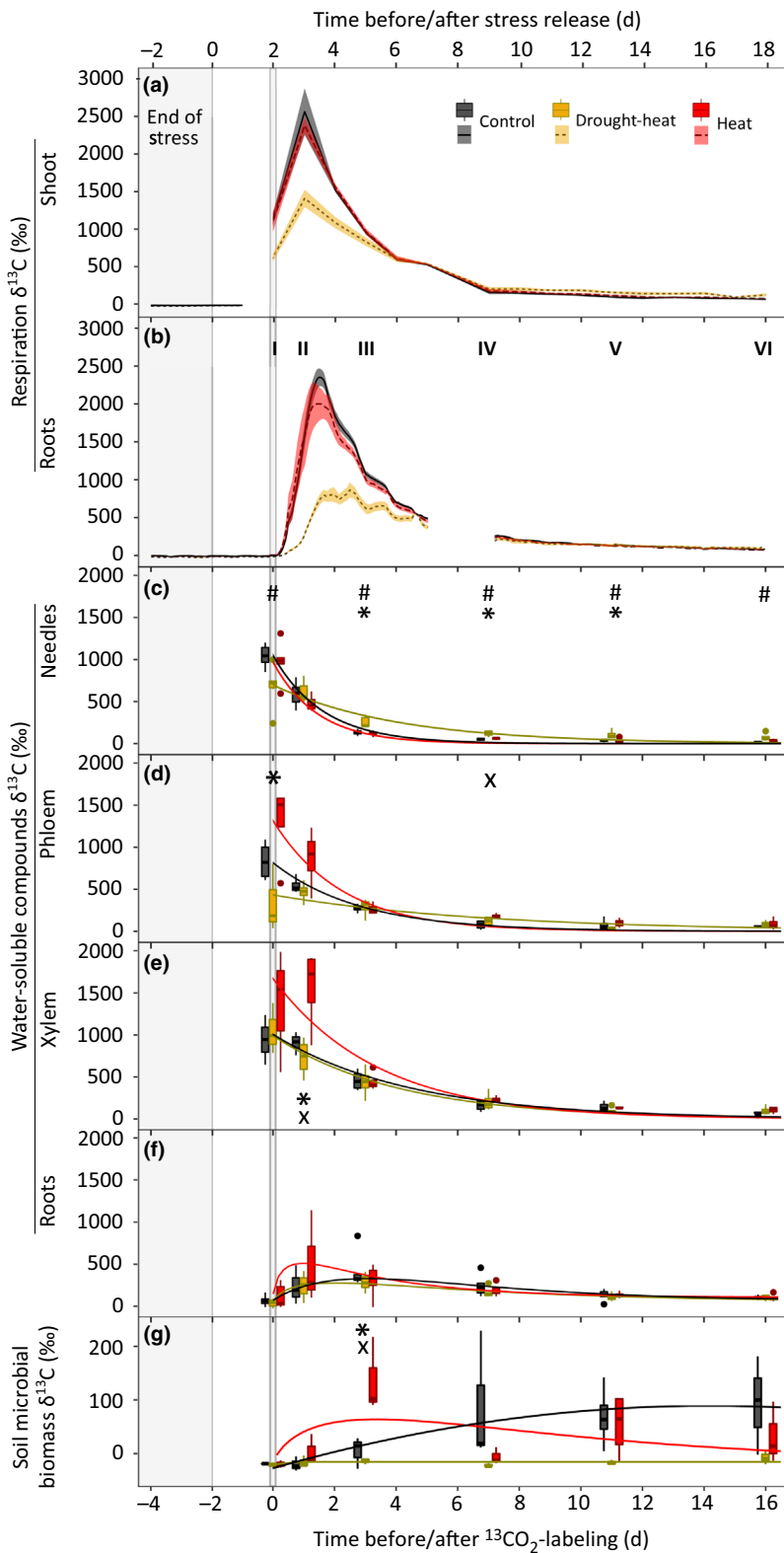
Fig. 4 Dynamics of $\delta^{13}C$ in respiration and biomass pools of Scots pine seedlings per treatment. Shown are treatment-specific $\delta^{13}C$ of (a) night-time averaged shoot respiration ($n = 6$), (b) hourly-averaged root respiration ($n = 6$), water-soluble compounds (WSC) in (c) needles, (d) branch phloem, (e) branch xylem and (f) roots ($n = 6$), as well as (g) soil microbial biomass ($n = 3$). In (a, b), data are treatment averages and shaded areas indicate $\pm$ SE. In (c–g), boxplots show the median, the 25th and 75th percentile, the most extreme data points (whiskers' extension) and the outliers as filled circles. The gray box represents the end of the stress period and the vertical gray line indicates $^{13}CO_2$ pulse-labeling 2 d after stress release. Tissue and soil sampling intervals following labeling are highlighted by roman letters (I–VI). Note that reported WSC and soil microbial biomass data on the pulse-labeling day are for samples taken 8 h after labeling start. Symbols indicate significant differences ($P < 0.05$) between treatments per sampling campaign (Kruskal–Wallis and Bonferroni *post hoc* test) as follows: drought-heat vs control (#), heat vs control (x), and drought-heat vs heat (*). The curve with the best fit is given per treatment (see Supporting Information Table S4).

Following heat release, tree C exchange recovered quickly in well-watered seedlings as shown previously (Ameye *et al.*, 2012; Ruehr *et al.*, 2019). Despite this nearly instantaneous recovery of C uptake and respiration, we found C allocation patterns to differ from control seedlings. Within 1 d after $^{13}CO_2$ labeling, we observed a preferential allocation of recent assimilates to water-soluble compounds (WSC) in phloem and xylem, and a tendency for faster C translocation to R_{root} in heat seedlings

Table 4 Mean residence time (MRT) and half-life time (HLT) of ^{13}C assimilated 2 d after stress release in respiration, different tissues and compounds of Scots pine seedlings.

| Organ/tissue	Flux/compound	Treatment	MRT (d)	HLT (d)	R^2
Shoot	Respiration	Control	2.3 (2.1, 2.5)	1.6 (1.4, 1.7)	0.90
		Heat	2.4 (2.3, 2.5)	1.7 (1.6, 1.8)	0.91
		Drought-heat	4.0 (3.7, 4.4)	2.8 (2.5, 3.0)	0.86
Roots	Respiration	Control	2.6 (2.4, 2.7)	1.8 (1.7, 1.9)	0.94
		Heat	2.7 (2.5, 2.9)	1.9 (1.7, 2.0)	0.93
		Drought-heat	4.9 (4.4, 5.4)	3.4 (3.1, 3.7)	0.85
Needles	WSC	Control	1.6 (1.4, 1.9)	1.1 (0.9, 1.3)	0.95
		Heat	1.4 (1.2, 1.8)	1.0 (0.8, 1.2)	0.83
		Drought-heat	4.0 (3.0, 5.8)	2.8 (2.1, 4.0)	0.89
Phloem	WSC	Control	2.8 (2.2, 3.9)	1.9 (1.5, 2.7)	0.79
		Heat	2.2 (1.5, 3.8)	1.6 (1.1, 2.6)	0.82
		Drought-heat	6.9 (4.2, 18.8)	4.8 (2.9, 13.0)	0.37
Xylem	WSC	Control	4.4 (3.5, 6.1)	3.1 (2.4, 4.3)	0.87
		Heat	3.4 (2.3, 6.1)	2.3 (1.6, 4.2)	0.88
		Drought-heat	4.1 (3.1, 6.2)	2.8 (2.1, 4.3)	0.84
Roots	WSC	Control	7.9 (5.3, 15.5)	5.5 (3.6, 10.7)	0.55
		Heat	7.6 (4.5, 24.8)	5.3 (3.1, 17.2)	0.52
		Drought-heat	10.5 (7.3, 18.8)	7.3 (5.0, 13.0)	0.58
Needles	Starch	Control	5.5 (3.5, 13.1)	3.8 (2.4, 9.1)	0.69
		Heat	0.6 (0.2, 1.6)	0.4 (0.2, 1.1)	0.72
		Drought-heat	6.6 (4.8, 10.7)	4.6 (3.3, 7.4)	0.79
Needles	Bulk	Control	1.5 (1.3, 1.8)	1.0 (0.9, 1.2)	0.62
		Heat	1.8 (1.4, 2.6)	1.3 (0.9, 1.8)	0.64
		Drought-heat	9.8 (7.0, 15.8)	6.8 (4.8, 10.9)	0.62
Phloem	Bulk	Control	6.1 (3.9, 13.3)	4.2 (2.7, 9.2)	0.35
		Heat	12.3 (7.4, 35.4)	8.5 (5.1, 24.5)	0.25
		Drought-heat	–	–	–

Values are derived following the $\delta^{13}C$ peak during a 16 d period after $^{13}CO_2$ pulse-labeling. The 95% confidence intervals are given in brackets, and R^2 of the fitted exponential decay function (Eqn 3) is indicated ($n = 6$ per treatment and time step for respiration, bulk and WSC; $n = 3$ for starch). MRT and HLT are only provided in case the fitted model was significant.

compared to the control (Fig. 4b,d,e). Based on the leakage-retrieval mechanism during phloem transport (van Bel, 2003; Thorpe *et al.*, 2005), sugars and other carbohydrates are released from phloem sieve tubes to feed the lateral sinks along the pathway, supporting tissue maintenance and growth (De Schepper *et al.*, 2013; Deslauriers *et al.*, 2014). Thus, the large ^{13}C signal in xylem WSC shortly post-heat could indicate support of secondary growth, consistent with ^{13}C allocation to branch cellulose 1 d after pulse-labeling (Fig. 5e). Additionally, a fast above–belowground coupling became evident in soil microbial biomass (SMB), where ^{13}C peaked 3 d postlabeling (Fig. 4g). C release via root exudates can support seedling growth indirectly via improved soil microbial functioning and nutrient cycling (Wagg *et al.*, 2014; Rennenberg & Dannenmann, 2015; Gessler *et al.*, 2017).

Heat combined with drought resulted in higher needle temperatures as a consequence of reduced evaporative cooling (Drake *et al.*, 2018), but we cannot tease apart the physiological impacts of this additional heating as our experimental set-up did not allow for a drought-only treatment. Generally, we found that the drought-heat treatment had profound impacts on tree C and water relations (see also Rehschuh & Ruehr, 2021). This was indicated by a strong reduction of respiration and stem diameter shrinkage (Fig. 3), consistent with previous studies (Ruehr *et al.*, 2016; Birami *et al.*, 2018). Hydraulic measurements further showed that stem hydraulic conductivity decreased by 25% under drought-heat (Rehschuh & Ruehr, 2021). These larger stress impacts, relative to the heat seedlings, were reflected in a much slower recovery of C cycling, stem growth and needle water potential (Ψ_{Needle}) with evident consequences for C allocation. A substantially longer mean residence time (MRT) and half-life time (HLT) of ^{13}C in needles and $R_{shoot\text{-}night}$ (Table 4) indicates a delayed translocation of recent C from source to sink organs. This likely originates from stress impacts on internal C transport via impaired phloem loading and/or reduced sink activity. Both could result in a passive overflow of NSC in aboveground organs, as observed here (Fig. 5). Impaired phloem functionality can reduce the source–sink coupling (Sevanto, 2014, 2018) under drought (Ruehr *et al.*, 2009; Blessing *et al.*, 2015; Hesse *et al.*, 2019) and postdrought (Zang *et al.*, 2014; Galiano *et al.*, 2017). Damage to the hydraulic system in drought-heat seedlings (Rehschuh & Ruehr, 2021) and a close link between xylem and phloem functioning (Hölttä *et al.*, 2009) supports impaired phloem functionality as underlying reason. This is further supported by shrinkage and slow expansion of stem diameter over 6 d, indicating rather slow hydration and repair of phloem sieve tubes.

Further, low sink activity might explain the reduced source–sink coupling. According to the pressure-flow hypothesis, phloem flow is driven by pressure differences between source and sink
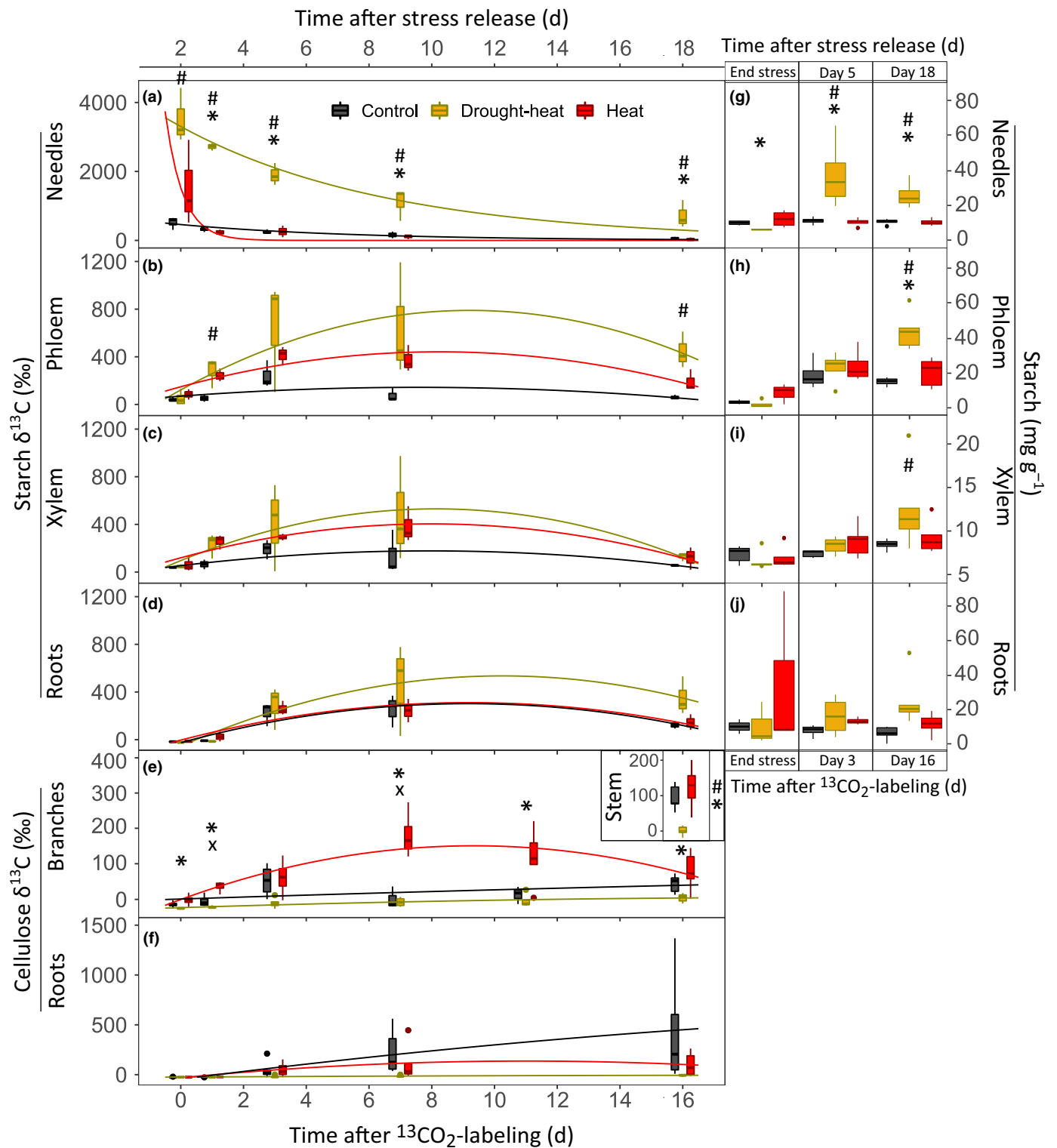
Fig. 5 Treatment-specific dynamics of $\delta^{13}C$ in starch and cellulose in tissues of Scots pine seedlings following $^{13}CO_2$ pulse-labeling (a–f), as well as starch concentrations at the end of stress and during recovery (g–k). Shown are $\delta^{13}C$ of starch in (a) needles, (b) branch phloem, (c) branch xylem and (d) roots (n = 3 per treatment), as well as of cellulose in (e) branches (phloem and xylem), stems (only 16 d after $^{13}CO_2$ labeling, see inserted panel) and (f) roots (n = 5–6 per treatment). Starch concentrations are depicted for (g) needles, (h) branch phloem, (i) branch xylem and (j) roots (n = 5–6 per treatment). Boxplots show the median, the 25th and 75th percentile, the most extreme data points (whiskers' extension) and the outliers as filled circles. Seedlings were $^{13}CO_2$ pulse-labeled on Day 0. Note that data on Day 0 are from sampling 8 h after the start of labeling. Symbols indicate significant differences ($P < 0.05$) between treatments within one sampling campaign (Kruskal–Wallis and Bonferroni *post hoc* test; drought-heat vs control (#), heat vs control (x), and drought-heat vs heat (*)). The regression with the best fit is depicted per treatment (see Supporting Information Table S4).
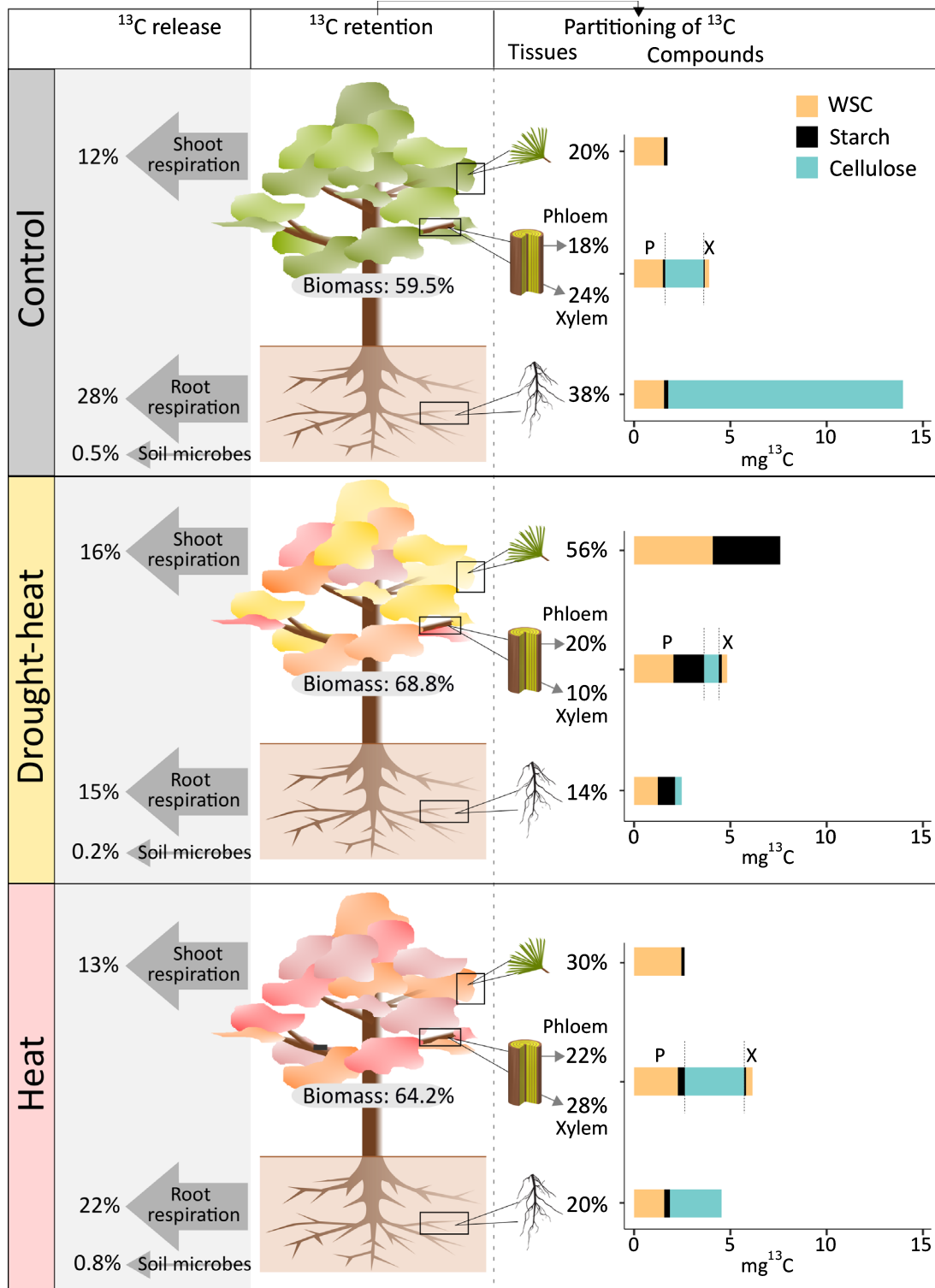
Fig. 6 Overview of treatment-specific carbon allocation during poststress recovery in *Pinus sylvestris* seedlings. The isotopic mass balance is based on ^{13}C uptake during $^{13}CO_2$ pulse-labeling, ^{13}C release (respiration and soil microbial biomass) and ^{13}C retention in tree biomass at the end of the recovery period, 18 d after stress release, that is, 16 d after pulse-labeling. Percentage of ^{13}C released is derived from total ^{13}C uptake relative to cumulative shoot and root respiration, and ^{13}C ingested by soil microbes (see Supporting Information Methods S6). Shoot respiration includes day- and night-time, whereas shoot day respiration was interpolated from shoot night respiration. Percent of ^{13}C retention in biomass was derived from ^{13}C release assuming a closed C balance. Additionally, the partitioning of ^{13}C between needles, xylem and phloem (including branches and stem), and roots is indicated (^{13}C partitioning – tissues), and the amount of label (in mg ^{13}C) allocated to water-soluble compounds (WSC), starch and cellulose in these tissues is shown (^{13}C partitioning – compounds). Note that compounds for woody xylem/phloem are depicted in one bar showing the amount of ^{13}C in WSC and starch separately (indicated as P, phloem and X, xylem), whereas the amount of ^{13}C in cellulose is shown for the entire stem/branch biomass. Also note that cellulose was not measured in needles, as seasonal needle elongation was completed.
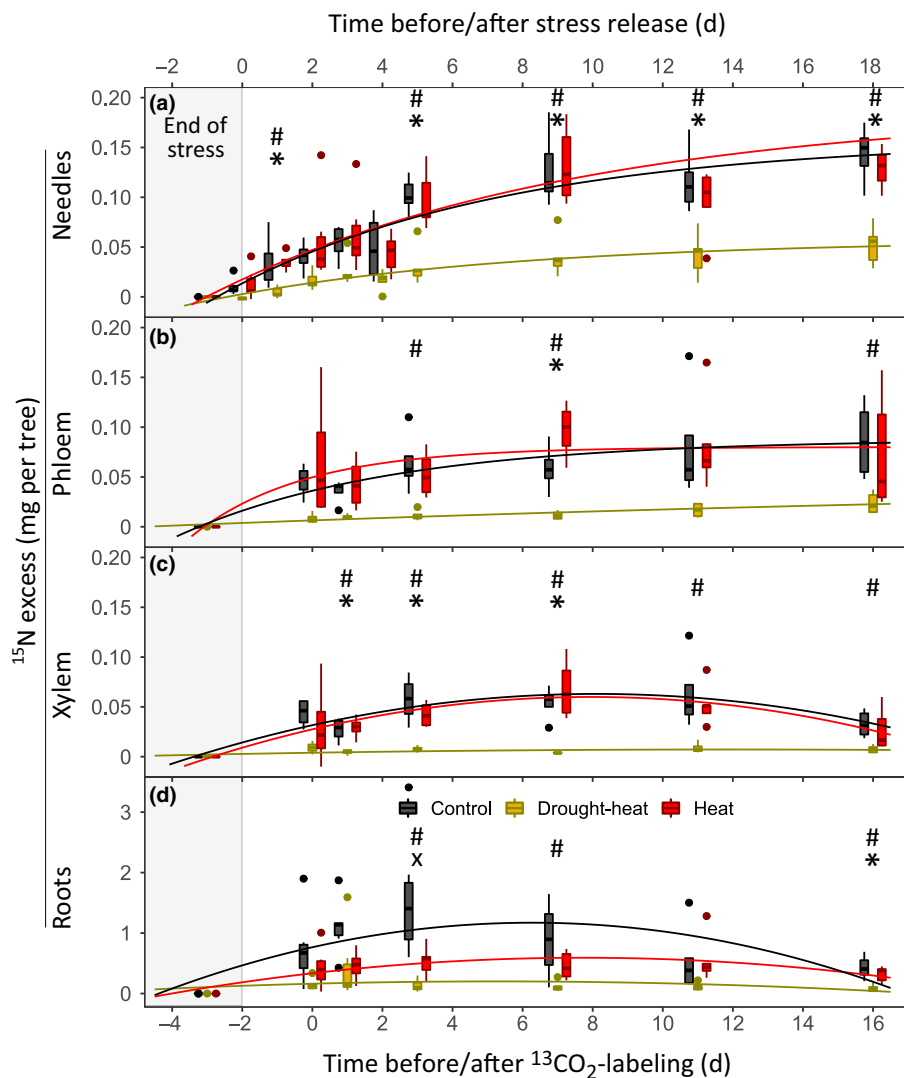
Fig. 7 Dynamics of ^{15}N excess of bulk material in (a) needles, (b) phloem, (c) xylem and (d) roots of Scots pine seedlings for the end of stress and the recovery period per treatment ($n = 6$). Boxplots show the median, the 25th and 75th percentile, the most extreme data points (whiskers' extension) and the outliers as closed circles. The gray box represents the end of the stress period, and the ^{15}N label was applied to the soil upon stress release (= 2 d before $^{13}CO_2$ pulse-labeling). Note that background values before stress release are also displayed. Tissue-specific biomass was determined at the end of the experiment, and ^{15}N excess in phloem and xylem includes branch and stem biomass. Symbols indicate significant differences ($P < 0.05$) between treatments per sampling campaign (Kruskal–Wallis and Bonferroni *post hoc* test) as follows: drought-heat vs control (#), heat vs control (x), and drought-heat vs heat (*). The curve with the best fit is given for each treatment (see Supporting Information Table S4).

tissues (Münch, 1930). If C demand for growth and maintenance is low in sink tissues, phloem transport will decrease, supported here by initially low secondary growth likely caused by drought-induced meristem inactivation and lower ^{13}C allocation to R_{root} (Figs 4b, 5e–f). Although limited C allocation to SMB has been reported under drought stress (Ruehr *et al.*, 2009; Hagedorn *et al.*, 2016; Joseph *et al.*, 2020), our findings are in contrast to Hagedorn *et al.* (2016) and Joseph *et al.* (2020), who reported enhanced C allocation to belowground sinks postdrought. Note that the timing of pulse-labeling after stress release might have an effect. In Hagedorn *et al.* (2016), ^{13}C pulse-labeling was conducted 14 d after re-wetting in beech seedlings, when soil respiration exceeded photosynthesis and the above–belowground coupling was fast. In our study, pulse-labeling was conducted 2 d after stress release, when the tree metabolism still appeared to operate in stress mode and phloem functionality was impaired. In summary, we can confirm our first hypothesis. In heat-treated seedlings C sink allocation was fast, whereas drought-heat stress delayed phloem translocation to belowground storage during early recovery.

Carbon allocation to storage, repair and growth

We found drought-heat but not heat seedlings to allocate significant amounts of C to starch during the entire recovery period (Figs 5, 6). This response most likely was triggered by drought impacts, as has been shown previously (Galiano *et al.*, 2017; Rehschuh *et al.*, 2020), but we cannot exclude an additional impact from high temperatures. Following excessive heating of coffee plants, accumulation of starch became visible alongside recovery of the damaged photosystem (Marias *et al.*, 2017), indicating that investment into storage might occur when a given stress-level caused functional imbalance. C stored in starch is a source for growth and dark respiration (Smith & Stitt, 2007), the latter conforming with peaks in night δ^{13}C of R_{root} in drought-heat seedlings. We suggest that shortly after stress release, C passively overflowed to storage due to reduced phloem translocation (see previous section) at the expense of growth (Figs 5e,f; Sala *et al.*, 2012; Dietze *et al.*, 2014; Galiano *et al.*, 2017). Later, c. 8 d after rewetting, when respiration rates had recovered, accumulating starch in branches and roots indicates a more active process

and underlines the importance of starch in tree fitness and survival (Thalmann & Santelia, 2017).

The dominant allocation of ^{13}C to starch in drought-heat seedlings resulted in a very low incorporation into root, branch and stem cellulose (Fig. 5e,f). In agreement, stem diameter remained below pre-stress values during the initial 6 d poststress, when a large fraction of ^{13}C had already been allocated. This was in stark contrast to heat seedlings, which upregulated aboveground woody growth immediately. The reasons could involve increased cambial activity and cell division under elevated temperatures, thus enhancing stem growth (Gričar et al., 2007; Gričar, 2013; Balducci et al., 2016). Despite the rather late seasonal timing of the experiment, the growing period was extended due to the simulation of summer day length and temperature. Growth is initiated by cell division, involving cellulose accumulation during the formation of new cell walls (Drakakaki, 2015). This step is followed by cell enlargement, wall thickening and secondary wall formation, involving intensive cellulose synthesis (Cuny et al., 2014, 2019). In our study, we suggest that heat enhanced cell division, yet once stress was released, cell enlargement continued, typically taking c. 9 d in Scots pine (Cuny et al., 2014).

In drought-heat seedlings, stem growth was accelerated in the second half of the recovery period. Hardly any ^{13}C detected in stem cellulose at the end of the experiment suggests that C skeletons for growth were supplied by older storage compounds including lipids, or from C assimilated after pulse-labeling. The delayed growth recovery agrees with the observed repair of cambial activity taking 2–4 wk post-drought-heat in *Picea mariana* saplings (Balducci et al., 2013). Enhanced stem growth promotes a re-establishment of the plant hydraulic system via new functional xylem (Trugman et al., 2018), yet repairing root functionality also would be highly important (Gao et al., 2021). In drought-heat seedlings, an upregulation of root-rhizosphere activity became apparent when R_{root} recovered at the end of the experiment. Based thereon, we suggest that during initial recovery, growth was limited by impaired phloem functioning, which repair enhanced the recovery of respiratory activity and growth later.

In summary, we partially refute our second hypothesis because short-term growth post-drought-heat was inhibited, whereas stem growth appeared to be a strong C sink only later on, concurrently with the recovery of above- and belowground respiration.

Coupling of C and N metabolism

Late season allocation preferences became apparent as control seedlings invested most ^{13}C into roots (Figs 5f, 6), alongside largest N uptake. This is consistent with roots as dominant C sink during the late growing season (Endrulat et al., 2010; Blessing et al., 2015), and N being invested into storage proteins that can be remobilized for growth in spring (Palacio et al., 2018). These phenological responses were altered by previous stress conditions. In recovering heat seedlings, large investments of C into branch and stem growth were consistent with enhanced allocation of N to aboveground tissues (Fig. 7; Rennenberg et al., 2006; Gessler et al., 2017). N uptake is operated at the whole-plant level by a cycling pool of N as a bidirectional exchange between the xylem and phloem within leaves, roots and the long-distance transport path (Gessler et al., 2004). This ensures the signaling of the actual N demand to regulate nutrient supply (Herschbach et al., 2012; Rennenberg & Dannenmann, 2015). Hence, the observed low N transport from below- to aboveground in drought-heat seedlings indicates a stress-induced inhibition of short-term growth (Fig. 7; Palacio et al., 2018). Moreover, low root N uptake post-drought-heat points towards stress-induced impairment of root functioning (Gaul et al., 2008).

The late seasonal timing of the experiment resulted in preferential belowground C allocation in control seedlings, which was not apparent in seedlings recovering from stress. A close coordination of C and N cycling poststress became apparent, confirming our third hypothesis. This was reflected in lower N uptake and aboveground allocation in recovering drought-heat seedlings as growth processes were not activated yet.

Conclusion

In well-watered Scots pine seedlings exposed to prolonged, but moderate daytime heat stress, C uptake and respiration recovered quickly. Accordingly, translocation of recent C to belowground was fast and woody growth – ^{13}C allocation to branch cellulose – was upregulated quickly. By contrast, combined heat and drought resulted in higher daytime leaf temperatures and substantially altered tree physiology and late season phenology, reflected in a delayed and reduced allocation of recent C to belowground following stress release. The underlying causes may include impaired phloem functioning and/or reduced C sink strength. This is consistent with a delayed increase of respiration, low ^{13}C allocation to cellulose and low N uptake during initial recovery. Later during recovery, stem diameter changes indicate enhanced secondary growth, not captured by the label.

The initially delayed translocation from source to sink organs following drought-heat release could have substantial consequences for tree functioning and nutrient uptake. If such a decoupling emerges relevant for forest regeneration, it should be considered in stress legacy modeling, while accounting for seasonality. To further elucidate the reversibility of stress damage and impairment of C and N cycling, we call for experiments addressing the impacts and timing of single and compound stressors during different recovery stages.

Author contributions

RR and NKR designed the study; RR conducted the experiment with support from AGast, SR, A-LJ and NKR; RR, A-LJ and SR conducted extractions for isotopic mass spectrometry and performed NSC analyses; RR analyzed the data with support from SR, MML and NKR; and RR wrote the original draft with reviewing and editing from NKR, SR, MML, AGessler and MS.

ORCID

Arthur Gessler https://orcid.org/0000-0002-1910-9589
Marco M. Lehmann https://orcid.org/0000-0003-2962-3351
Romy Rehschuh https://orcid.org/0000-0001-9140-0306
Nadine K. Ruehr https://orcid.org/0000-0001-5989-7463
Matthias Saurer https://orcid.org/0000-0002-3954-3534

Data availability

The gas-exchange and isotopic data will be made available through PANGAEA® Data Publisher for Earth & Environmental Science. Other data will be made available upon request.

References

Aaltonen H, Lindén A, Heinonsalo J, Biasi C, Pumpanen J. 2017. Effects of prolonged drought stress on Scots pine seedling carbon allocation. *Tree Physiology* 37: 418–427.

Ameye M, Wertin TM, Bauweraerts I, McGuire MA, Teskey RO, Steppe K. 2012. The effect of induced heat waves on *Pinus taeda* and *Quercus rubra* seedlings in ambient and elevated CO_2 atmospheres. *New Phytologist* 196: 448–461.

Anderegg WRL, Schwalm C, Biondi F, Camarero JJ, Koch G, Litvak M, Ogle K, Shaw JD, Shevliakova E, Williams AP *et al.* 2015. Pervasive drought legacies in forest ecosystems and their implications for carbon cycle models. *Science* 349: 528–532.

Balducci L, Cuny HE, Rathgeber CBK, Deslauriers A, Giovannelli A, Rossi S. 2016. Compensatory mechanisms mitigate the effect of warming and drought on wood formation. *Plant, Cell & Environment* 39: 1338–1352.

Balducci L, Deslauriers A, Giovannelli A, Rossi S, Rathgeber CBK. 2013. Effects of temperature and water deficit on cambial activity and woody ring features in *Picea mariana* saplings. *Tree Physiology* 33: 1006–1017.

Bauweraerts I, Ameye M, Wertin TM, McGuire MA, Teskey RO, Steppe K. 2014. Water availability is the decisive factor for the growth of two tree species in the occurrence of consecutive heat waves. *Agricultural and Forest Meteorology* 189: 19–29.

van Bel AJE. 2003. Phloem transport: the collective power of single modules. In: Larcher W, ed. *Physiological plant ecology*. New York, NY, USA: Springer, 151–155.

Birami B, Bamberger I, Ghirardo A, Grote R, Arneth A, Gaona-Colmán E, Nadal-Sala D, Ruehr NK. 2021. Heatwave frequency and seedling death alter stress-specific emissions of volatile organic compounds in Aleppo pine. *Oecologia*. doi: 10.1007/s00442-021-04905-y.

Birami B, Gattmann M, Heyer AG, Grote R, Arneth A, Ruehr NK. 2018. Heat waves alter carbon allocation and increase mortality of Aleppo pine under dry conditions. *Frontiers in Forests and Global Change* 1: e1285.

Birami B, Nägele T, Gattmann M, Preisler Y, Gast A, Arneth A, Ruehr NK. 2020. Hot drought reduces the effects of elevated CO_2 on tree water-use efficiency and carbon metabolism. *New Phytologist* 226: 1607–1621.

Blessing CH, Werner RA, Siegwolf R, Buchmann N. 2015. Allocation dynamics of recently fixed carbon in beech saplings in response to increased temperatures and drought. *Tree Physiology* 35: 585–598.

Buras A, Schunk C, Zeiträg C, Herrmann C, Kaiser L, Lemme H, Straub C, Taeger S, Gößwein S, Klemmt H-J *et al.* 2018. Are Scots pine forest edges particularly prone to drought-induced mortality? *Environmental Research Letters* 13: 025001.

Burnham K, Anderson D. 2002. *Model selection and multi-model inference*. New York, NY, USA: Springer.

Coumou D, Robinson A, Rahmstorf S. 2013. Global increase in record-breaking monthly-mean temperatures. *Climate Change* 118: 771–782.

Cuny HE, Fonti P, Rathgeber CBK, Arx G, Peters RL, Frank DC. 2019. Couplings in cell differentiation kinetics mitigate air temperature influence on conifer wood anatomy. *Plant, Cell & Environment* 42: 1222–1232.

Cuny HE, Rathgeber CBK, Frank D, Fonti P, Fournier M. 2014. Kinetics of tracheid development explain conifer tree-ring structure. *New Phytologist* 203: 1231–1241.

Dannenmann M, Bimüller C, Gschwendtner S, Leberecht M, Tejedor J, Bilela S, Gasche R, Hanewinkel M, Baltensweiler A, Kögel-Knabner I *et al.* 2016. Climate change impairs nitrogen cycling in European beech forests. *PLoS ONE* 11: e0158823.

Dannoura M, Maillard P, Fresneau C, Plain C, Berveiller D, Gerant D, Chipeaux C, Bosc A, Ngao J, Damesin C *et al.* 2011. In situ assessment of the velocity of carbon transfer by tracing ^{13}C in trunk CO_2 efflux after pulse labelling: variations among tree species and seasons. *New Phytologist* 190: 181–192.

De Boeck HJ, Dreesen FE, Janssens IA, Nijs I. 2010. Climatic characteristics of heat waves and their simulation in plant experiments. *Global Change Biology* 16: 1992–2000.

De Schepper V, De Swaef T, Bauweraerts I, Steppe K. 2013. Phloem transport: a review of mechanisms and controls. *Journal of Experimental Botany* 64: 4839–4850.

Deslauriers A, Beaulieu M, Balducci L, Giovannelli A, Gagnon MJ, Rossi S. 2014. Impact of warming and drought on carbon balance related to wood formation in black spruce. *Annals of Botany* 114: 335–345.

Dietze MC, Sala A, Carbone MS, Czimczik CI, Mantooth JA, Richardson AD, Vargas R. 2014. Nonstructural carbon in woody plants. *Annual Review of Plant Biology* 65: 667–687.

Drakakaki G. 2015. Polysaccharide deposition during cytokinesis: challenges and future perspectives. *Plant Science* 236: 177–184.

Drake JE, Furze ME, Tjoelker MG, Carrillo Y, Barton CVM, Pendall E. 2019. Climate warming and tree carbon use efficiency in a whole-tree $^{13}CO_2$ tracer study. *New Phytologist* 222: 1313–1324.

Drake JE, Tjoelker MG, Vårhammar A, Medlyn B, Reich PB, Leigh A, Pfautsch S, Blackman CJ, López R, Aspinwall MJ *et al.* 2018. Trees tolerate an extreme heatwave via sustained transpirational cooling and increased leaf thermal tolerance. *Global Change Biology* 24: 2390–2402.

Dyckmans J, Flessa H. 2001. Influence of tree internal N status on uptake and translocation of C and N in beech: a dual ^{13}C and ^{15}N labeling approach. *Tree Physiology* 21: 395–401.

Endrulat T, Saurer M, Buchmann N, Brunner I. 2010. Incorporation and remobilization of ^{13}C within the fine-root systems of individual *Abies alba* trees in a temperate coniferous stand. *Tree Physiology* 30: 1515–1527.

Epron D, Bahn M, Derrien D, Lattanzi FA, Pumpanen J, Gessler A, Hogberg P, Maillard P, Dannoura M, Gerant D *et al.* 2012. Pulse-labelling trees to study carbon allocation dynamics: a review of methods, current knowledge and future prospects. *Tree Physiology* 32: 776–798.

Fotelli MN, Rienks M, Rennenberg H, Geßler A. 2004. Climate and forest management affect ^{15}N-uptake, N balance and biomass of European beech seedlings. *Trees* 18: 157–166.

Fuentes L, Duguy B, Nadal-Sala D. 2018. Short-term effects of spring prescribed burning on the understory vegetation of a *Pinus halepensis* forest in Northeastern Spain. *Science of the Total Environment* 610: 720–731.

Galiano L, Timofeeva G, Saurer M, Siegwolf R, Martínez-Vilalta J, Hommel R, Gessler A. 2017. The fate of recently fixed carbon after drought release: towards unravelling C storage regulation in *Tilia platyphyllos* and *Pinus sylvestris*. *Plant, Cell & Environment* 40: 1711–1724.

Gao D, Josep J, Werner RA, Brunner I, Zürcher A, Hug C, Wang A, Zhao C, Bai E, Meusburger K *et al.* 2021. Drought alters the carbon footprint of trees

in soils—tracking the spatio-temporal fate of ^{13}C-labelled assimilates in the soil of an old-growth pine forest. *Global Change Biology* 27: 2491–2506.

Gattmann M, Birami B, Nadal Sala D, Ruehr NK. 2020. Dying by drying: timing of physiological stress thresholds related to tree death is not significantly altered by highly elevated CO_2. *Plant, Cell & Environment* 44: 356–370.

Gaul D, Hertel D, Borken W, Matzner E, Leuschner C. 2008. Effects of experimental drought on the fine root system of mature Norway spruce. *Forest Ecology and Management* 56: 1151–1159.

Gessler A, Jung K, Gasche R, Papen H, Heidenfelder A, Börner E, Metzler B, Augustin S, Hildebrand E, Rennenberg H. 2005. Climate and forest management influence nitrogen balance of European beech forests: microbial N transformations and inorganic N net uptake capacity of mycorrhizal roots. *European Journal of Forest Research* 124: 95–111.

Gessler A, Kopriva S, Rennenberg H. 2004. Regulation of nitrate uptake at the whole-tree level: interaction between nitrogen compounds, cytokinins and carbon metabolism. *Tree Physiology* 24: 1313–1321.

Gessler A, Schaub M, McDowell NG. 2017. The role of nutrients in drought-induced tree mortality and recovery. *New Phytologist* 214: 513–520.

Giri A, Heckathorn S, Mishra S, Krause C. 2017. Heat stress decreases levels of nutrient-uptake and-assimilation proteins in tomato roots. *Plants* 6: 6.

Gričar J. 2013. Influence of temperature on cambial activity and cell differentiation in *Quercus Sessiliflora* and *Acer Pseudoplatanus* of different ages. *Drvna Industrija* 64: 95–105.

Gričar J, Zupančič M, Čufar K, Oven P. 2007. Regular cambial activity and xylem and phloem formation in locally heated and cooled stem portions of Norway spruce. *Wood Science and Technology* 41: 463–475.

Grossiord C, Buckley TN, Cernusak LA, Novick KA, Poulter B, Siegwolf RTW, Sperry JS, McDowell NG. 2020. Plant responses to rising vapor pressure deficit. *New Phytologist* 226: 1550–1566.

Hagedorn F, Joseph J, Peter M, Luster J, Pritsch K, Geppert U, Kerner R, Molinier V, Egli S, Schaub M et al. 2016. Recovery of trees from drought depends on belowground sink control. *Nature Plants* 2: 1–5.

Hao Z, AghaKouchak A, Phillips TJ. 2013. Changes in concurrent monthly precipitation and temperature extremes. *Environmental Research Letters* 8: 034014.

Herschbach C, Gessler A, Rennenberg H. 2012. Long-distance transport and plant internal cycling of N- and S-compounds. In: Lüttge U, Beyschlag W, Büdel B, Francis D, eds. *Progress in botany, Vol. 73*. Berlin, Germany: Springer, 161–188.

Hesse BD, Goisser M, Hartmann H, Grams TEE. 2019. Repeated summer drought delays sugar export from the leaf and impairs phloem transport in mature beech. *Tree Physiology* 39: 192–200.

Hölttä T, Mencuccini M, Nikinmaa E. 2009. Linking phloem function to structure: analysis with a coupled xylem–phloem transport model. *Journal of Theoretical Biology* 259: 325–337.

IPCC. 2018. Summary for policymakers. In: *Special Report: Global Warming of 1.5°C*. [WWW document] URL https://www.ipcc.ch/sr15/chapter/spm/ [accessed 23 October 2021].

Jaime L, Batllori E, Margalef-Marrase J, Pérez Navarro MÁ, Lloret F. 2019. Scots pine (*Pinus sylvestris* L.) mortality is explained by the climatic suitability of both host tree and bark beetle populations. *Forest Ecology and Management* 448: 119–129.

Jarvi MP, Burton AJ. 2013. Acclimation and soil moisture constrain sugar maple root respiration in experimentally warmed soil. *Tree Physiology* 33: 949–959.

Joseph J, Gao D, Backes B, Bloch C, Brunner I, Gleixner G, Haeni M, Hartmann H, Hoch G, Hug C et al. 2020. Rhizosphere activity in an old-growth forest reacts rapidly to changes in soil moisture and shapes whole-tree carbon allocation. *Proceedings of the National Academy of Sciences, USA* 117: 24885–24892.

Klein D, Schulz C. 2011. Wälder und Holzprodukte als Kohlenstoffspeicher. *LWF Aktuell* 85: 40–43.

Kumarathunge DP, Drake JE, Tjoelker MG, López R, Pfautsch S, Vårhammar A, Medlyn BE. 2020. The temperature optima for tree seedling photosynthesis and growth depend on water inputs. *Global Change Biology* 26: 2544–2560.

Kuznetsova A, Brockhoff PB, Christensen RHB. 2017. LMERTEST package: tests in linear mixed effects models. *Journal of Statistical Software* 82: 1–26.

Lalonde S, Tegeder M, Throne-Holst M, Frommer WB, Patrick JW. 2003. Phloem loading and unloading of sugars and amino acids. *Plant, Cell & Environment* 26: 37–56.

Landhäusser SM, Chow PS, Dickman LT, Furze ME, Kuhlman I, Schmid S, Wiesenbauer J, Wild B, Gleixner G, Hartmann H et al. 2018. Standardized protocols and procedures can precisely and accurately quantify non-structural carbohydrates. *Tree Physiology* 38: 1764–1778.

Laumer W, Andreu L, Helle G, Schleser GH, Wieloch T, Wissel H. 2009. A novel approach for the homogenization of cellulose to use micro-amounts for stable isotope analyses. *Rapid Communications in Mass Spectrometry* 23: 1934–1940.

Le Quéré C, Andrew RM, Friedlingstein P, Sitch S, Hauck J, Pongratz J, Pickers PA, Korsbakken JI, Peters GP, Canadell JG et al. 2018. Global carbon budget 2018. *Earth System Science Data* 10: 2141–2194.

Lehmann MM, Rinne KT, Blessing C, Siegwolf RTW, Buchmann N, Werner RA. 2015. Malate as a key carbon source of leaf dark-respired CO_2 across different environmental conditions in potato plants. *Journal of Experimental Botany* 66: 5769–5781.

Lenth RV. 2017. Using lsmeans. *Journal of Statistical Software* 69: 1–33.

Lenth R, Singmann H, Love J, Buerkner P, Herve M. 2020. EMMEANS: estimated marginal means, aka least-squares means. R package v.1.5.0. [WWW document] URL https://github.com/rvlenth/emmeans.

Marias DE, Meinzer FC, Still C. 2017. Impacts of leaf age and heat stress duration on photosynthetic gas exchange and foliar nonstructural carbohydrates in *Coffea arabica*. *Ecology and Evolution* 7: 1297–1310.

Martínez-Vilalta J, Sala A, Asensio D, Galiano L, Hoch G, Palacio S, Piper FI, Lloret F. 2016. Dynamics of non-structural carbohydrates in terrestrial plants: a global synthesis. *Ecological Monographs* 86: 495–516.

McDowell NG, Allen CD, Anderson-Teixeira K, Aukema BH, Bond-Lamberty B, Chini L, Clark JS, Dietze M, Grossiord C, Hanbury-Brown A et al. 2020. Pervasive shifts in forest dynamics in a changing world. *Science* 368: eaaz9463.

McDowell N, Pockman WT, Allen CD, Breshears DD, Cobb N, Kolb T, Plaut J, Sperry J, West A, Williams DG et al. 2008. Mechanisms of plant survival and mortality during drought: why do some plants survive while others succumb to drought? *New Phytologist* 178: 719–739.

Millard P, Grelet G-A. 2010. Nitrogen storage and remobilization by trees: ecophysiological relevance in a changing world. *Tree Physiology* 30: 1083–1095.

Münch E. 1930. *Die Stoffbewegungen in der Pflanze*. Jena, Germany: Gustav Fischer.

Palacio S, Camarero JJ, Maestro M, Alla AQ, Lahoz E, Montserrat-Martí G. 2018. Are storage and tree growth related? Seasonal nutrient and carbohydrate dynamics in evergreen and deciduous Mediterranean oaks. *Trees* 32: 777–790.

Pan Y, Birdsey RA, Fang J, Houghton R, Kauppi PE, Kurz WA, Phillips OL, Shvidenko A, Lewis SL, Canadell JG et al. 2011. A large and persistent carbon sink in the world's forests. *Science* 333: 988–993.

R Core Team. 2019. *R: a language and environment for statistical computing*. R package v.3.6.1. Vienna, Austria: R Foundation for Statistical Computing.

Rehschuh R, Cecilia A, Zuber M, Faragó T, Baumbach T, Hartmann H, Jansen S, Mayr S, Ruehr N. 2020. Drought-induced xylem embolism limits the recovery of leaf gas exchange in Scots pine. *Plant Physiology* 184: 852–864.

Rehschuh R, Ruehr NK. 2021. Unrevealing water and carbon relations during and after heat and hot drought stress in *Pinus sylvestris*. *bioRxiv*. doi: 10.1101/2021.06.29.450316.

Rennenberg H, Dannenmann M. 2015. Nitrogen nutrition of trees in temperate forests- the significance of nitrogen availability in the pedosphere and atmosphere. *Forests* 6: 2820–2835.

Rennenberg H, Loreto F, Polle A, Brilli F, Fares S, Beniwal RS, Gessler A. 2006. Physiological responses of forest trees to heat and drought. *Plant Biology* 8: 556–571.

Richter A, Wanek W, Werner RA, Ghashghaie J, Jäggi M, Gessler A, Brugnoli E, Hettmann E, Göttlicher SG, Salmon Y et al. 2009. Preparation of starch and soluble sugars of plant material for the analysis of carbon isotope composition: a comparison of methods. *Rapid Communications in Mass Spectrometry* 23: 2476–2488.

Ruehr NK, Gast A, Weber C, Daub B, Arneth A. 2016. Water availability as dominant control of heat stress responses in two contrasting tree species. *Tree Physiology* 36: 164–178.

Ruehr NK, Grote R, Mayr S, Arneth A. 2019. Beyond the extreme: recovery of carbon and water relations in woody plants following heat and drought stress. *Tree Physiology* 39: 1285–1299.

Ruehr NK, Offermann CA, Gessler A, Winkler JB, Ferrio JP, Buchmann N, Barnard RL. 2009. Drought effects on allocation of recent carbon: from beech leaves to soil CO_2 efflux. *New Phytologist* 184: 950–961.

Sage RF, Way DA, Kubien DS. 2008. Rubisco, Rubisco activase, and global climate change. *Journal of Experimental Botany* 59: 1581–1595.

Sala A, Woodruff DR, Meinzer FC. 2012. Carbon dynamics in trees: feast or famine? *Tree Physiology* **32**: 764–775.

Salomón RL, De Roo L, Bodé S, Boeckx P, Steppe K. 2021. Efflux and assimilation of xylem-transported CO_2 in stems and leaves of tree species with different wood anatomy. *Plant, Cell & Environment* **44**: 3494–3508.

Schönbeck L, Li M-H, Lehmann MM, Rigling A, Schaub M, Hoch G, Kahmen A, Gessler A. 2020. Soil nutrient availability alters tree carbon allocation dynamics during drought. *Tree Physiology* **41**: 697–707.

Schrader SM, Wise RR, Wacholtz WF, Ort DR, Sharkey TD. 2004. Thylakoid membrane responses to moderately high leaf temperature in Pima cotton. *Plant, Cell & Environment* **27**: 725–735.

Schuldt B, Buras A, Arend M, Vitasse Y, Beierkuhnlein C, Damm A, Gharun M, Grams TEE, Hauck M, Hajek P *et al.* 2020. A first assessment of the impact of the extreme 2018 summer drought on Central European forests. *Basic and Applied Ecology* **45**: 86–103.

Sevanto S. 2014. Phloem transport and drought. *Journal of Experimental Botany* **65**: 1751–1759.

Sevanto S. 2018. Drought impacts on phloem transport. *Current Opinion in Plant Biology* **43**: 76–81.

Smith AM, Stitt M. 2007. Coordination of carbon supply and plant growth. *Plant, Cell & Environment* **30**: 1126–1149.

Stéfanon M, Drobinski P, D'Andrea F, Lebeaupin-Brossier C, Bastin S. 2014. Soil moisture-temperature feedbacks at meso-scale during summer heat waves over Western Europe. *Climate Dynamics* **42**: 1309–1324.

Teskey R, Wertin T, Bauweraerts I, Ameye M, Mcguire MA, Steppe K. 2015. Responses of tree species to heat waves and extreme heat events: tree response to extreme heat. *Plant, Cell & Environment* **38**: 1699–1712.

Thalmann M, Santelia D. 2017. Starch as a determinant of plant fitness under abiotic stress. *New Phytologist* **214**: 943–951.

Thorpe MR, Minchin PEH, Gould N, McQueen JC. 2005. The stem apoplast: a potential communication channel in plant growth regulation. In: Holbrook NM, Zwieniecki MA, eds. *Vascular transport in plants*. Oxford, UK: Academic Press, 201–220.

Timofeeva G, Treydte K, Bugmann H, Rigling A, Schaub M, Siegwolf R, Saurer M. 2017. Long-term effects of drought on tree-ring growth and carbon isotope variability in Scots pine in a dry environment. *Tree Physiology* **37**: 1028–1041.

Trugman AT, Detto M, Bartlett MK, Medvigy D, Anderegg WRL, Schwalm C, Schaffer B, Pacala SW. 2018. Tree carbon allocation explains forest drought-kill and recovery patterns. *Ecology Letters* **21**: 1552–1560.

Tyree MT, Sperry JS. 1989. Vulnerability of xylem to cavitation and embolism. *Annual Review of Plant Biology* **40**: 19–36.

Vance ED, Brookes PC, Jenkinson DS. 1987. An extraction method for measuring soil microbial biomass C. *Soil Biology and Biochemistry* **19**: 703–707.

Wagg C, Bender SF, Widmer F, van der Heijden MGA. 2014. Soil biodiversity and soil community composition determine ecosystem multifunctionality. *Proceedings of the National Academy of Sciences, USA* **111**: 5266–5270.

Zang U, Goisser M, Grams TEE, Haberle K-H, Matyssek R, Matzner E, Borken W. 2014. Fate of recently fixed carbon in European beech (*Fagus sylvatica*) saplings during drought and subsequent recovery. *Tree Physiology* **34**: 29–38.

Supporting Information

Additional Supporting Information may be found online in the Supporting Information section at the end of the article.

Fig. S1 Soil moisture during the pre-stress drought period.

Fig. S2 Environmental conditions for Weißenburg–Emetzheim.

Fig. S3 Relative humidity during the tree chamber experiment.

Fig. S4 $\delta^{13}C$ in root respiration during the 4-h $^{13}CO_2$ labeling pulse.

Fig. S5–S8 Dynamics in ^{13}C excess of tissue compounds and soil microbial biomass.

Fig. S9 Nonstructural carbohydrate dynamics.

Fig. S10–S11 Dynamics in ^{13}C excess and $\delta^{13}C$ of bulk material.

Fig. S12 Cumulative fluxes of respired ^{13}C.

Fig. S13 Dynamics of the N content.

Methods S1 Implementation of heat-drought scenarios.

Methods S2 Tree gas exchange chambers.

Methods S3 NSC analysis.

Methods S4 Extraction of WSC, starch and cellulose.

Methods S5 Soil microbial biomass extraction.

Methods S6 Isotope ratio mass spectrometry.

Table S1 Pre-defined maximum air temperatures.

Table S2 Background values for $\delta^{13}C$.

Table S3 Results of linear-mixed effects models.

Table S4 Functions and percentages explained by best-fit models for fitted curves.

Please note: Wiley Blackwell are not responsible for the content or functionality of any Supporting Information supplied by the authors. Any queries (other than missing material) should be directed to the *New Phytologist* Central Office.